Intracellular Osteopontin Promotes the Release of TNFα by Mast Cells to Restrain Neuroendocrine Prostate Cancer

Roberta Sulsenti[1], Giuseppina B. Scialpi[1], Barbara Frossi[2], Laura Botti[1], Renata Ferri[1], Irene Tripodi[1], Annamaria Piva[1], Sabina Sangaletti[1], Davide Pernici[1], Valeria Cancila[3], Francesco Romeo[4], Claudia Chiodoni[1], Daniele Lecis[1], Francesca Bianchi[5], Irene Fischetti[1], Claudia Enriquez[1], Filippo Crivelli[6], Marco Bregni[6], Giuseppe Renne[7], Salvatore Pece[4], Claudio Tripodo[3], Carlo E. Pucillo[2], Mario P. Colombo[1], and Elena Jachetti[1]

ABSTRACT

Neuroendocrine prostate cancer (NEPC) is an aggressive form of prostate cancer that emerges as tumors become resistant to hormone therapies or, rarely, arises *de novo* in treatment-naïve patients. The urgent need for effective therapies against NEPC is hampered by the limited knowledge of the biology governing this lethal disease. Based on our prior observations in the transgenic adenocarcinoma of the mouse prostate (TRAMP) spontaneous prostate cancer model, in which the genetic depletion of either mast cells (MC) or the matricellular protein osteopontin (OPN) increases NEPC frequency, we tested the hypothesis that MCs can restrain NEPC through OPN production, using *in vitro* co-cultures between murine or human tumor cell lines and MCs, and *in vivo* experiments. We unveiled a role for the intracellular isoform of OPN, so far neglected compared with the secreted isoform. Mechanistically, we unraveled that the intracellular isoform of OPN promotes TNFα production in MCs via the TLR2/TLR4-MyD88 axis, specifically triggered by the encounter with NEPC cells. We found that MC-derived TNFα, in turn, hampered the growth of NEPC. We then identified the protein syndecan-1 (SDC1) as the NEPC-specific TLR2/TLR4 ligand that triggered this pathway. Interrogating published single-cell RNA-sequencing data, we validated this mechanism in a different mouse model. Translational relevance of the results was provided by *in silico* analyses of available human NEPC datasets and by immunofluorescence on patient-derived adenocarcinoma and NEPC lesions. Overall, our results show that MCs actively inhibit NEPC, paving the way for innovative MC-based therapies for this fatal tumor. We also highlight SDC1 as a potential biomarker for incipient NEPC.

Introduction

Prostate cancer is still one of the leading cancer-related causes of death among men (1). Advanced and metastatic tumors are treated with androgen deprivation therapy (ADT), but its efficacy is limited, as tumors become castration resistant (CRPC). Androgen receptor pathway inhibitors (ARPI), such as enzalutamide, can be an option for treating CRPC. However, prognosis remains dismal due to existing or acquired resistance. Therapeutic resistance to ADT/ARPI relies on cellular plasticity that, in a relevant fraction of patients, gives rise to tumors endowed with neuroendocrine features, defined as treatment-related neuroendocrine prostate cancer (t-NEPC; ref. 2). This fatal prostate cancer variant can occur "*de novo*" in untreated patients, but this is a rare occurrence (3). Treatment-related and *de novo* NEPC share a common transcriptional profile (3), suggesting that, regardless of their origin, common pathways exist in the two conditions. Investigating such common pathways can provide insights toward the identification of new therapeutic targets.

The paucity of distinct genomic aberrations and the dysregulation of epigenetic and transcription factors in NEPC suggest that the tumor microenvironment can govern its development (4). MCs are innate immune cells endowed with diverse immunomodulatory properties, capable of exerting both positive and negative effects on cancer progression (5). The impact of MCs on tumor development varies depending on the tumor type, signals originating from the tumor microenvironment, and the interactions of MCs with other immune cells (5). We have previously shown that MCs accumulate within prostate adenocarcinoma favoring its growth, by providing MMP9 at the initial stages (6), and by inhibiting the antitumor immune response (7). Conversely, we found that MCs are excluded from NEPC in both

[1]Molecular Immunology Unit, Department of Experimental Oncology, Fondazione IRCCS Istituto Nazionale dei Tumori di Milano, Milan, Italy. [2]Immunology Section, Department of Medicine, University of Udine, Udine, Italy. [3]Tumor Immunology Unit, Department of Health Sciences, University of Palermo, Palermo, Italy. [4]Dipartimento di Onologia Sperimentale, European Institute of Oncology IRCCS, Milan, Italy. [5]Microenvironment and Biomarkers in Solid tumors Unit, Fondazione IRCCS Istituto Nazionale dei Tumori di Milano, Milan, Italy. [6]Oncology-Hematology Unit, ASST Valle Olona, Busto Arsizio, Italy. [7]Uropathology and Intraoperative Diagnostic Division, European Institute of Oncology IRCCS, Milan, Italy.

Current address for A. Piva: Department of Experimental Oncology, IEO, European Institute of Oncology IRCCS, Milan, Italy; current address for F. Bianchi: Department of Biomedical Science for Health, University of Milan, Italy and Laboratorio Morfologia Umana Applicata, IRCCS Policlinico San Donato, Milan, Italy; and current address for C. Enriquez: Lymphoid Organ Development and Function Unit, IRCCS San Raffaele Hospital, Milan, Italy.

Corresponding Author: Elena Jachetti, Molecular Immunology Unit, Department of Experimental Oncology, Fondazione IRCCS Istituto Nazionale Tumori di Milano, via Amadeo, Milano 42 20133, Italy. E-mail: elena.jachetti@istitutotumori.mi.it

Cancer Immunol Res 2024;12:1147–69

doi: 10.1158/2326-6066.CIR-23-0792

mouse and human tumor samples (6) and that the genetic or pharmacological inhibition of MCs increases NEPC incidence in the TRAMP mouse model (8). Likewise, in TRAMP mice rendered knockout for the protein osteopontin (OPN), we observed an increase in NEPC frequency (9), which prompted us to hypothesize that MCs can protect from NEPC by producing OPN.

OPN is a nonstructural extracellular matrix protein with critical roles in the cross-talk between cancer cells and the tumor microenvironment, being involved in proliferation, invasion, and metastasis (10). OPN exists in two main isoforms, one secreted (sOPN) by the cell and one retained into the cytoplasm (iOPN), resulting from an alternative translation initiation site of the same transcript (11). Despite intense investigation of the role of sOPN in the immune system and tumor biology, the activity of iOPN is less well characterized and, so far, to our knowledge, it is totally unexplored in MCs and in prostate cancer (12). Of note, iOPN has been identified as an adaptor protein, able to bind MyD88 (13, 14) and to either stimulate or inhibit the signaling downstream of several toll-like receptors (TLR), namely, TLR2, TLR4, and TLR9, depending on the cell type and on the specific TLR engaged (13–16).

In this study, we uncovered a role for MC-produced iOPN in enhancing TLR2/TLR4 signaling and leading to increased TNFα production, which subsequently restrains the growth of NEPC. Furthermore, we identified syndecan-1 (SDC1) as the specific molecule expressed by NEPC cells, which was responsible for triggering TNFα production in MCs. These findings can be exploited to design innovative MC-based immunotherapy for the treatment of NEPC and suggest SDC1 as a biomarker for the detection of emerging NEPC.

Materials and Methods

Mice and treatments

TRAMP mice on the C57BL6/J background (C57BL/6-tgN(TRAMP)8247Ng; RRID:IMSR_JAX:003135) were kindly provided by Dr. Vincenzo Bronte (Verona University Hospital, Italy), under agreement with Dr. Norman Michael Greenberg (formerly at Fred Hutchinson Cancer Research Center, Seattle, WA, USA). They were maintained heterozygous and screened as described previously (17). Because TRAMP mice are paired in heterozygosity, half of the progeny do not carry the oncogene and are therefore wild-type C57BL6 mice (hereafter named WT mice). OPN knockout B6.129S6(Cg)-Spp1tm1Blh/J ($OPN^{-/-}$; RRID: IMSR_JAX:004936) mice were purchased from The Jackson Laboratories and crossed more than 12 generations with TRAMP mice, in order to obtain congenic B6.tgN (TRAMP)8247Ng Spp1<tm1Blh>/J ($OPN^{-/-}$TRAMP). Mice deficient in MCs [C57BL/6-KitW-sh/W-sh (Kit^{Wsh}; ref. 18)] were purchased from The Jackson Laboratories and crossed more than 12 generations with TRAMP mice, to obtain MC-deficient B6.tgN (TRAMP) 8247Ng KitW-sh/W-sh mice (Kit^{Wsh}-TRAMP). Mice deficient for *Sparc* on a mixed 129SV/C57BL/6 background (RRID:IMSR_JAX:003728; ref. 19) were provided by C. Howe (The Wistar Institute, Philadelphia, PA, USA). They were crossed to C57BL/6 for 12 generations (Charles River Laboratories; RRID: SCR_003792) and then crossed more than 12 generations with TRAMP mice [B6.tgN (TRAMP)8247Ng Sparc<tm1Hwe> Ptprc<a>/J] to generate $SPARC^{-/-}$ TRAMP mice.

Male $TRAMP^{+/-}$, $OPN^{-/-}$ $TRAMP^{+/-}$, Kit^{Wsh}-$TRAMP^{+/-}$, and $SPARC^{-/-}$ $TRAMP^{+/-}$ mice were used for experiments. WT mice were used as bone marrow donors for the preparation of MCs (as described in "Bone marrow–derived MC differentiation *in vitro*").

Experiments were performed in male $TRAMP^{+/-}$, $OPN^{-/-}TRAMP^{+/-}$ or Kit^{Wsh}-$TRAMP^{+/-}$ mice. Surgical castration was executed in 20-week-old TRAMP mice, under anesthesia with ketamine (100 mg/kg; Imalgene, Boeringher Ingheilm) and xilazine (5 mg/kg; Rompun, Bayer). Carprofene (5 mg/kg; Norocarp, Norbrook) was given as analgesic after recovery postanesthesia. For reconstitution experiments, 5×10^6 bone marrow–derived MCs (BMMC), obtained as described in "Bone marrow–derived MC differentiation *in vitro*," were injected intraperitoneally (i.p.) into 8-week-old Kit^{Wsh}-TRAMP mice. All experimental mice were followed until 25 to 30 weeks of age and then euthanized to collect prostates for histologic evaluation. Animal housing and experimentation were performed in accordance with Italian law (D.lgs 26/2014), and *in vivo* experiments were approved by the Italian Ministry of Health (project 74312.35, authorization number 185/2021-PR).

Bone marrow–derived MC differentiation *in vitro*

BMMCs were obtained by *in vitro* differentiation of bone marrow cells obtained by flushing femora and tibiae of WT, $OPN^{-/-}$, $MyD88^{-/-}$, or $TNF\alpha^{-/-}$ mice. Bones of $MyD88^{-/-}$ mice were kindly provided by Prof. Luigina Romani, from the University of Perugia. The bone marrow flushing of $TNF\alpha^{-/-}$ mice (B6;129S-Tnftm1Gkl/J, purchased from The Jackson Laboratories) had been previously collected and stored in our lab at −180°C in a freezing medium containing 10% of DMSO (Sigma Aldrich) and 90% of fetal bovine serum (FBS; Gibco). Bone marrow precursors were cultured *in vitro* in RPMI-1640 (Gibco) supplemented with 20% FBS, 200-U/m penicillin (Cambrex), 150-U/mL streptomycin, 10-mmol/L Hepes, 10-mmol/L sodium pyruvate, 2-mmol/L L-glutamine, and 5-mmol/L β-mercaptoethanol (all Gibco), in the presence of 20 ng/mL of IL3 (Peprotech, cat. n. AF-213-13), and SCF (Peprotech, cat. n. AF-250-03). After 4 weeks of culture, BMMCs were monitored for FcεRI and c-Kit expression by flow cytometry and used if purity was more than 95% (Supplementary Fig. S1). Except when it is specifically indicated that MC/9 or HMC1 cell lines were used, BMMCs were used for all *in vitro* and *in vivo* experiments, and for brevity we always define them as MCs.

Cell lines and *in vitro* experiments

T1525, T23, and ST4787 cell lines were isolated in our laboratory from TRAMP mice and have been previously characterized (6, 20). TC566 and TC411K cells were isolated from NEPC arising in two different TRAMP mice subjected to surgical castration. Briefly, the tumors were digested with 1-mg/mL collagenase I (Gibco) for 2 hours at 37°C, and recovered cells were plated to establish the new cell lines. TC566 and TC411K cells were characterized for expression NEPC of markers as shown below. No other authentication method was performed. The human cell lines 22Rv1 (ATCC cat. n. CRL-2505, RRID: CVCL_1045, purchased in 2018), LASCPC-01 (ATCC cat. n. CRL-3356, RRID: CVCL_UE17, purchased in 2022), and NCI-H660 (ATCC cat. n. CRL-5813, RRID: CVCL_1576, purchased in 2021) cells were purchased from ATCC and not further authenticated. Murine tumor cells were cultured in DMEM (Gibco) supplemented with 10% FBS (Gibco), 200-U/mL penicillin (Cambrex), 150-U/mL streptomycin, 10-mmol/L Hepes, 10-mmol/L sodium pyruvate, nonessential amino acid mixture, and 2-mmol/L L-glutamine (all Gibco). 22Rv1 cells were cultured in RPMI-1640 (Gibco) supplemented with 10% FBS (Gibco), 200-U/mL penicillin (Cambrex), 150-U/mL streptomycin, 10-mmol/L sodium pyruvate, 2-mmol/L L-glutamine (all Gibco), and 2.5 g/L of D-(+)-glucose

(Sigma Aldrich). Human NEPC cells (LASCPC-01 and NCI-H660) were cultured in modified Hites medium composed of RPMI-1640 (Gibco) supplemented with 5% FBS (Gibco), 200-U/mL penicillin (Cambrex), 150-U/mL streptomycin, 4-mmol/L L-glutamine (both Gibco), 5-μg/mL insulin, 10-nmol/L hydrocortisone, 0.01-mg/mL transferrin, 30-nmol/L sodium selenite, and 10-nmol/L β-estradiol (all Sigma Aldrich).

The murine MC/9 MC cell line (ATCC cat. n. CRL-8306, RRID: CVCL_0408; ref. 21) was purchased from ATCC. The human HMC1 cell line (RRID: CVCL_0003; ref. 22) was kindly provided by Dr. Juan Rivera (NIH, Bethesda, MD, USA). MC/9 cells were cultured in DMEM (Gibco) supplemented with 10% FBS (Gibco), 200-U/mL penicillin (Cambrex), 150-U/mL streptomycin, 10-mmol/L Hepes, 10-mmol/L sodium pyruvate, nonessential amino acid mixture 2-mmol/L L-glutamine, and 5-mmol/L β-mercaptoethanol (all Gibco), in the presence of 20 ng/mL of IL3 (Peprotech, cat. n. AF-213-13). HMC1 cells were cultured in RPMI-1640 (Gibco) supplemented with 10% FBS (Gibco), 200-U/mL penicillin (Cambrex), 150-U/mL streptomycin, and 10-mmol/L sodium pyruvate (all Gibco).

All cell lines were routinely tested for Mycoplasma using the MicoAlert Mycoplasma Detection Kit (Lonza, cat n. LT07-118). For experiments, all cells were used within a maximum of five passages since thawing.

For *in vitro* experiments, tumor cells and MCs were plated in six-well or 12-well plates (50,000 or 100,000 cells/well, respectively), either alone or in co-culture at a 1:1 ratio, for 4 days. In dedicated experiments, six-well transwell plates (0.4-μm pore size) were used to divide cancer cells (seeded in the bottom of the well) and MCs (seeded in the top chamber). When indicated, a neutralizing monoclonal antibody against TNFα (10 μg/mL, rat anti-mouse, clone V1q, purified from hybridoma cells as indicated in Supplementary Table S1, which lists all the antibodies used in this study), recombinant TNFα (20, 50, or 100 ng/mL; Peprotech, cat n. AF-315-01A), recombinant IL1β (20, 50, or 100 ng/mL; Peprotech, cat n. AF-211-11B), an inhibitor of NF-κB (BAY 11-7082, 10 μmol/L; Merk, cat n. B5556), an inhibitor of MEK (PD98059, 10 μmol/L; Merk, cat n. 513001), an inhibitor of TLR4 (TAK-242, 100 nmol/L; Calbiochem, cat n. 243984-11-4) or an inhibitor of TLR2 (TL2-C29, 50 μg/mL; InvivoGen, cat n. inh-c29) were added. In murine co-cultures, tumor cell growth was evaluated by trypan blue count, as they grow in adhesion and were thus distinguished by MCs that grow in suspension. In human co-cultures, tumor cell growth was evaluated by flow cytometry count.

Histopathological evaluation of mouse prostates

TRAMP prostate lesions were scored according to histopathological and immunophenotypical analyses as previously described (7, 23). Formalin-fixed paraffin-embedded (FFPE) prostate samples were cut into 5-μm sections. For histopathology, slides were deparaffined, rehydrated, stained with hematoxylin and eosin (BioOptica), and then evaluated by a board-certified pathologist (C. Tripodo). On serial slides, immunofluorescence for adenocarcinoma (CK8) and NEPC (SYP) markers were performed (see "Immunofluorescence and immunohistochemistry"). Prostate lesions were classified as follows: (i) high-grade intraepithelial neoplasia (HGPIN): high-grade prostatic intraepithelial neoplasia, characterized by CK8 expression; (ii) ADENO: adenocarcinoma characterized by CK8 positive atypical cells forming distorted/ill-defined glands within the stroma; and (iii) NEPC: composed of sheets and nests of medium-sized to large cells with high nuclear to cytoplasmic ratio and/or anaplastic morphology. Cells were immunoreactive for SYP and either negative (in case of pure small-cell NEPC) or positive for CK8 (in case of tumors with mixed adenocarcinoma and NEPC features; ref. 24). When NEPC areas and ADENO lesions were present in different lobes, the tumor was classified as NEPC.

Human prostate cancer samples

FFPE human prostatectomies, from patients either untreated or who underwent neoadjuvant ADT, were obtained from ASST Valle Olona, Busto Arsizio (VA), Italy (Protocol number 0046679/18), and from the European Institute of Oncology, Milan, Italy, respectively (authorization number UID 2133). All samples were collected in accordance with the Helsinki Declaration; informed written consent was not obtained because according to institutional rules, it was not necessary for these analyses. Samples collected post-ADT were scored as NEPC based on the expression of SYP and CgA, as shown in ref. 23; in this study in particular we analyzed samples from #PT1, PT2, PT4, PT6, PT13, and PT14 of ref. 23. Tissue collection, fixation, and processing were performed according to standardized protocols as part of routine clinical activity. Immunofluorescence and immunohistochemistry performed in this study, are described below (see "Immunofluorescence and immunohistochemistry") and were approved by the Institutional Review Boards of ASST Valle Olona and European Institute of Oncology (Protocol number 0046679/18 and UID 2133, respectively).

Lentiviral vectors and viral supernatant preparation

Lentiviral vectors containing the sequences encoding either for mouse OPNf or iOPN were obtained by cloning the OPNf sequence (from pUC57-Spp1 plasmid, DBA Italia) or the iOPN sequence (kindly provided to our laboratory by Prof. Mari L. Shinohara, Duke University School of Medicine, Durham, NC, USA) into the lentiviral backbone pLVX-EF1a-IRES-ZsGreen1 (Takarabio, cat. n. 631982). The empty pLVX-EF1a-IRES-ZsGreen1 vector was used as control.

The production of lentiviral particles was performed using a third-generation packaging system involving the transfection of 293T producer cells. 5×10^6 cells were seeded in 150 mm plates using Iscove's IMDM (Lonza) with 10% FBS and, the day after, a co-transfection using $CaCl_2$ was carried out with three packaging plasmids: pMDLg/pRRE (quantity used 16.25 μg), pRSV-REV (quantity used 6.25 μg), pMD2-VSV-G (quantity used 8.75 μg), and the plasmid with the gene of interest (OPNf or iOPN; quantity used 25 μg). After 24 hours, the supernatant was removed, and a fresh medium was added. The next day supernatants containing viral particles were collected, centrifuged at 1,500 rpm for 5 minutes to exclude residual cells, and passed through a 0.45 μm filter.

Overexpression of OPNf and iOPN in MC/9 cells

In 12-well plates, 5×10^6 MC/9 cells were seeded and incubated with viral supernatants (0.75 mL of viral supernatant in 2 mL of total medium). After 24 hours, the medium was changed and, 4 days later, the percentage of infected cells was assessed by evaluating ZsGreen1 positivity by flow cytometry. After *in vitro* expansion, ZsGreen1$^+$ cells were sorted by FACS to obtain a pure population. Immunofluorescence and ELISA for OPN were performed to confirm the expression of the protein.

Flow cytometry

For surface staining of tumor cells or MCs, single-cell suspensions were incubated with the desired antibodies for 15 minutes at 4°C and then washed in PBS supplemented with 2% FBS. For intracellular detection of TNFα, brefeldin A (5 μg/mL; Sigma Aldrich cat. n. B7651) was added for 4 hours, and then, cells were stained with surface antibodies to CD49f and CD45 to distinguish cancer cells and MC populations, respectively. Cells were then fixed with IC Fixation Buffer and permeabilized with Permeabilization Buffer according to the Intracellular Fixation & Permeabilization Set protocol (Thermo Fisher Scientific, cat. n. 88-8824). Finally, the samples were stained with anti-TNFα for 20 minutes at 4°C. All samples were acquired with a BD LSRII Fortessa instrument and analyzed with the FlowJo software (version 10.10.0). All the antibodies used in flow cytometry are listed in Supplementary Table S1.

Cytospin

Cells were suspended at 10^5/100 μL in PBS. Glass slides were mounted with a paper pad and cuvettes with a metal holder, loaded with 100 μL of cell suspension, and then spun for 2 minutes at 2,000 rpm with a cytocentrifuge. After detaching of cuvettes and filters, slides were dried overnight and then fixed for 15 minutes with PBS containing 4% paraformaldehyde. After permeabilization for 10 minutes with PBS containing 0.1% Triton X-100 (Sigma Aldrich), sections were incubated with 0.1-mol/L glycine (Sigma Aldrich) for 5 minutes at room temperature. Then, sections were blocked with PBS containing Tween-20 (0.1%, Sigma Aldrich) or, for MCs and MC/9, with PBS containing 10% FBS and 5-μg/mL FC blocking (Anti-Mouse CD16/CD32 monoclonal antibody, Invitrogen, cat. n. 14-0161-86), and we followed the protocol described below for the immunofluorescence.

Immunofluorescence and immunohistochemistry

All primary and secondary antibodies used for immunofluorescence are listed in Supplementary Table S1.

For the detection of OPN in MCs and MC/9 *in vitro*, we added wheat germ agglutinin (WGA) in the medium for 15 minutes at 37°C before proceeding to cytospins and immunofluorescence staining. Then, after the blocking, slides derived from cytospins were stained with primary antibody for 1.5 hours at room temperature and, after washing with PBS, staining was revealed using a specific secondary antibody for 30 minutes at room temperature. Nuclei were highlighted with 4′,6-diamidino-2-phenylindole (DAPI; ThermoFisher, cat. n. D1306) for 10 minutes at room temperature. Cover glasses were mounted using ProLong Gold antifade reagent (Invitrogen, cat. n. P36934). Fluorescent images were acquired with a confocal laser-scanning microscope Leica TCS SP8 × (Leica Microsystems) equipped with a pulsed super-continuum White Light Laser (470–670 nm; 1 nm tuning step size). Laser lines were 495 nm for FITC and Alexa 488, and 556 nm for Alexa 555. Detection ranges were 501 to 556 nm and 569 to 630 nm, respectively. Images were acquired in the scan format 1,024 × 1,024 pixels using an HC PL APO 62X/1.40 CS2 oil immersion objective and a pinhole set to 1 airy unit. Data were analyzed using the software Leica LASX rel.1.1 (Leica Microsystems). Images were mounted using the ImageJ 2 (RRID: SCR003070), software.

For the detection of CK8, SYP, TRY, OPN, TNFα, and SDC1, FFPE sections (5 μm) of murine and human tumor samples were de-paraffined and rehydrated. For double detection of CK8/SYP, TRY/TNFα, or TRY/OPN in murine samples and for the detection of SDC1 and CGA, antigen retrieval was performed utilizing the Novocastra Epitope Retrieval Solution pH 9 (Novocastra, Leica Biosystem) and autoclaving at 95°C for 15 minutes. For the double detection of TRY/TNFα in human samples, antigen retrieval was performed utilizing the Novocastra Epitope Retrieval Solution pH 6 (Novocastra, Leica Biosystem) and autoclaving at 95°C for 15 minutes. For the double detection of TRY and OPN in human samples, antigen retrieval was performed utilizing the Novocastra Epitope Retrieval Solution pH 6 (Novocastra, Leica Biosystem) in a thermostatic bath at 98°C for 30 minutes.

Sections were brought to room temperature and washed with PBS. Then, sections were blocked with PBS containing Tween-20 (0.1%, Sigma Aldrich) and 5% BSA (Sigma Aldrich) or, for evaluation of OPN in human samples, with 0.4% casein in PBS (Novocastra, Leica Biosystem). Sections were incubated with OPN and TRY primary antibodies for 1.5 hours at room temperature, with CgA primary antibody for 3 hours, and with CK8, SYP, TNFα, or SDC1 primary antibodies overnight at 4°C. When necessary, secondary antibodies were added for 30 minutes at room temperature. Nuclei were highlighted with DAPI (ThermoFisher, cat. n. D1306) for 10 minutes at room temperature. Cover glasses were mounted using ProLong Gold antifade reagent (Invitrogen, cat. n. P36934). Images were acquired with a Leica DM4 B microscope equipped with a Leica DFC450 C digital camera, utilizing the LAS X software. Images were mounted using the ImageJ 2 software. The quantification of TRY/TNFα cells in murine tumor samples was performed with the ImageJ 2 software. For the quantification of TRY/TNFα cells in human samples, whole slide images were acquired using a NanoZoomer S60 Digital slide scanner (Hamamatsu Photonics K.K.) with a 20×/0.75 NA dry objective. The signal intensity quantification analysis was completed in QuPath (v0.4.2; RRID: SCR018257): nuclei segmentation on the DAPI channel was achieved using the StarDist extension with an in-house trained deep-learning model; then, the cytoplasmic cell area was segmented considering a 3-μm-thick band around each nucleus; a custom classifier was trained to identify tryptase-positive cells that were then considered for the subsequent analyses. Tables containing the mean intensity values in the cytoplasmic compartment of each cell for each stained marker were extracted from QuPath and further analyzed using RStudio (v2023.03.0).

For the evaluation of infiltrating MCs in mouse and human tumor samples, FFPE sections (5 μm) sections were stained with toluidine blue (BioOptica).

ELISA

OPN in culture supernatants was detected using the DuoSet ELISA Kit (R&D System, cat. n. DY441) according to the manufacturer's protocol. Optical densities were determined on a microplate reader Tecan Spark (Tecan; RRID: SCR_021897).

Multiple immunoassay

Custom ProcartaPlex Multiplex Immunoassay (ThermoFisher Scientific) plates were used to evaluate a pool of 19 murine cytokines and chemokines in supernatants derived from co-cultures between cancer cells and MCs. Samples were incubated in a 96-well plate with polystyrene magnetic beads coated with small molecule-specific antibodies and then exposed to detection antibodies. Samples were incubated with streptavidin-PE and a reading buffer was added. The plate was red in a Luminex reader (Bio-Plex-200, Bio-Rad, RRID: SCR_018026). The concentration of each analyte

bounded to its specific magnetic bead corresponds to the mean fluorescent intensity of the reporter signal.

Western blot

Cells were lysed on ice for 30 minutes using RIPA buffer (25-mmol/L Tris-HCl pH 7.4, 150-mmol/L NaCl, 1% NP40, 0.5% DOC, 0.1% SDS, 1-mmol/L Na_3VO_4, 1-mmol/L phenylmethylsulfonylfluoride) with phosphatase (PhosSTOP, Roche, cat. n. 4906845001) and protease (cOmplete, Roche cat. n. 11836153001) inhibitor cocktails. Lysates were then centrifuged at 13,000 rpm for 20 minutes and the supernatants were stored at −80°C. Proteins were quantified through Pierce BCA Protein Assay Kit (Thermofisher, cat. n. 23225), and optical density was evaluated using a Spark Multimode microplate reader (RRID: SCR_021897). Lysates (25–30 ng/sample) were run on NuPAGE Bis-Tris gels (4%–12% polyacrylamide; Invitrogen, Thermo Fisher Scientific) and transferred on polyvinylidene difluoride (PVDF) membrane (GE Healthcare). The membrane was blocked in TBS with 0.1% Tween® 20 detergent (20-mmol/L Tris-base pH 7.6, 150-mmol/L NaCl, 0.1% Tween-20) containing 5% BSA for 1 hour at room temperature. Then, the membrane was incubated overnight at 4°C with the desired primary antibody. After washing, the membrane was incubated with horseradish peroxidase (HRP)–conjugated secondary antibody for 1 hour at room temperature. All primary and secondary antibodies used for western blot are listed in Supplementary Table S1. Staining was revealed with Western BLoT Hyper HRP Substrate (Takara, cat. n. T7103A) or ECL Star Enhanced Chemiluminescent Substrate (Euroclone, cat. n. EMP001005) and either developed on an X-ray film or acquired with the Azure 600 Western Blot Imaging System (Azure Biosystems, Cat. n. AZI600, RRID: SCR_023780). Digital quantification of staining intensity was performed with the ImageJ software and reported as normalized intensities relative to internal control (β-actin or vinculin).

Immunoprecipitation

For 30 minutes, 7×10^6 WT or $OPN^{-/-}$ MCs were stimulated with lipopolysaccharide (1 μg/mL; Sigma cat. n. L4130) + lipoteichoic acid (10 μg/mL; InvivoGen Cat. n. tlrl-pslta). Then, cells were lysed with 400 μL of RIPA lysis buffer containing 50-mmol/L NaF, 1-mmol/L phenylmethylsulfonylfluoride, 1-mmol/L Na_3VO_4, and a protease inhibitor cocktail (Sigma Aldrich). Cellular extracts were pre-cleared with 5 μL of prewashed protein A/G-agarose beads (Pierce Classic Magnetic IP/Co-IP Kit Cat. n. 88804) for 10 minutes at room temperature and then incubated with 7 μL of rabbit anti-MyD88 (Cell Signaling, clone D80F5 cat. n. 4283, RRID: AB_10547882) at 4°C for 18 hours on a rotator; 50 μL of 50% slurry of prewashed protein A/G-agarose beads was then added to each sample, followed by incubation for an additional 1 hour at room temperature. The samples were washed four times in lysis buffer, solubilized in Laemmli buffer, and subjected to Western blot analyses. Images were acquired using the Odyssey CLx (LI-COR Biosciences, RRID: SCR_014579). Antibodies used are listed in Supplementary Table S1.

siRNA transient transfection

ST4787 cells were seeded in six-well plates and transfected with 10 μmol/L of mouse siRNA (ThermoFisher Scientific) specific for *Cd14*, *Sdc1*, *Anxa2*, *Hspa2*, or a negative control (scramble; ThermoFisher Scientific) using Lipofectamine RNAiMAX Transfection reagent (ThermoFisher Scientific, cat. n. 13778075) according to the manufacturer protocol. After 72 hours, ST4787 cells were recovered and tested by flow cytometry or western blot for CD14, SDC1, ANXA2, and HSPA2 protein expression. Two different sequences of siRNA were used to perform the silencing of every gene. All the assay IDs for the siRNA are listed in Supplementary Table S2.

Real-time PCR

Total RNA from cells was extracted using the Quick-RNA microprep kit (Zymo Research, cat n. R1051), and its purity and yield were assessed using a NanoDrop 2000c spectrophotometer (ThermoFisher Scientific); 500 ng of RNA were reverse transcribed using the High-Capacity cDNA Reverse Transcription Kit (ThermoFisher Scientific, cat n. 4368814). Real-time PCR was performed in a total volume of 20 μL using the Taqman Fast Universal PCR Master Mix no Amperase UNG (ThermoFisher Scientific, cat. n. 4352042), 20 ng of cDNA, and specific Taqman probes. To evaluate the expression of the 29 genes candidate for binding to TLR2/TLR4 we used Custom TaqMan Array Plates (ThermoFisher Scientific, cat. n. 4413259; custom configuration 3 × 32), performing the experiment according to the manufacturer's protocol. All the assays were run on a QuantStudio 3 instrument (RRID: SCR_018712). Values were normalized to internal control (*Gapdh*) using the 2^-ΔCT method. All probes used are listed in Supplementary Table S2.

Microarray analysis on mouse NEPC

We collected adenocarcinoma ($n = 7$) or incipient NEPC ($n = 7$) samples from TRAMP or $SPARC^{-/-}$TRAMP mice, respectively. The latter are prone to NEPC differentiation, as we previously described (23). Total RNA was extracted using Qiazol reagent (Qiagen cat. n. 79306) and purified with the RNeasy kit (Qiagen cat. n. 74104) on a QIAcube automated station (Qiagen) according to the manufacturer's instructions. The quantity and quality of the extracted RNA were determined with the 4200 TapeStation system (Agilent, RRID:SCR_019398) and Qubit Fluorometer (ThermoFisher, RRID:SCR_020553), respectively. The Clariom S assay (Affymetrix) was used for gene expression profiling. Raw data were preprocessed using the sst-RMA algorithm implemented in the Transcriptome Analysis Console software (Thermo Fisher, RRID: SCR_018718) and analyzed using the R software (R Core Team). Data were deposited in the Gene Expression Omnibus (GEO) database (GSE242811).

Analyses of human and mouse datasets

Median normalized RNA-sequencing (RNA-seq) data of the human Beltran data set, including 34 CRPC and 15 NEPC samples (25) were downloaded from c-BioPortal (26, 27) and imported into R software (R Core Team). The *z*-scores data were filtered for the genes composing the MC signature (*Hpgds*, *Atp8b4*, *Stxbp6*, *Rab27b*, *Bmp2k*, *Adrb2*, *Stxbp6*, *Enpp3*, *Il3*, *Crisp3*, and *Cma1*; ref. 7), and the gene mean was calculated for every sample. Boxplot representation of the mean expression of the MC gene signature in CRPC-ADENO and CRPC-NEPC classes was performed and the adjusted *P* value between the two groups was calculated using the Wilcoxon–Mann–Whitney test with Benjamini & Hochberg (FDR) correction. Class comparison between CRPC and NEPC samples (25), was performed with the *limma* R package (28), and consequently, gene set enrichment analysis (GSEA) was performed with the *fGSEA* R package with HALLMARK gene set, based on the normalized enrichment scale.

The RNA-seq data from the Labrecque dataset (29) and the metadata containing the association between the samples and the five phenotypic groups (ARPC, AR^+/NE^-; AMPC, AR^+/NE^+; ARLPC,

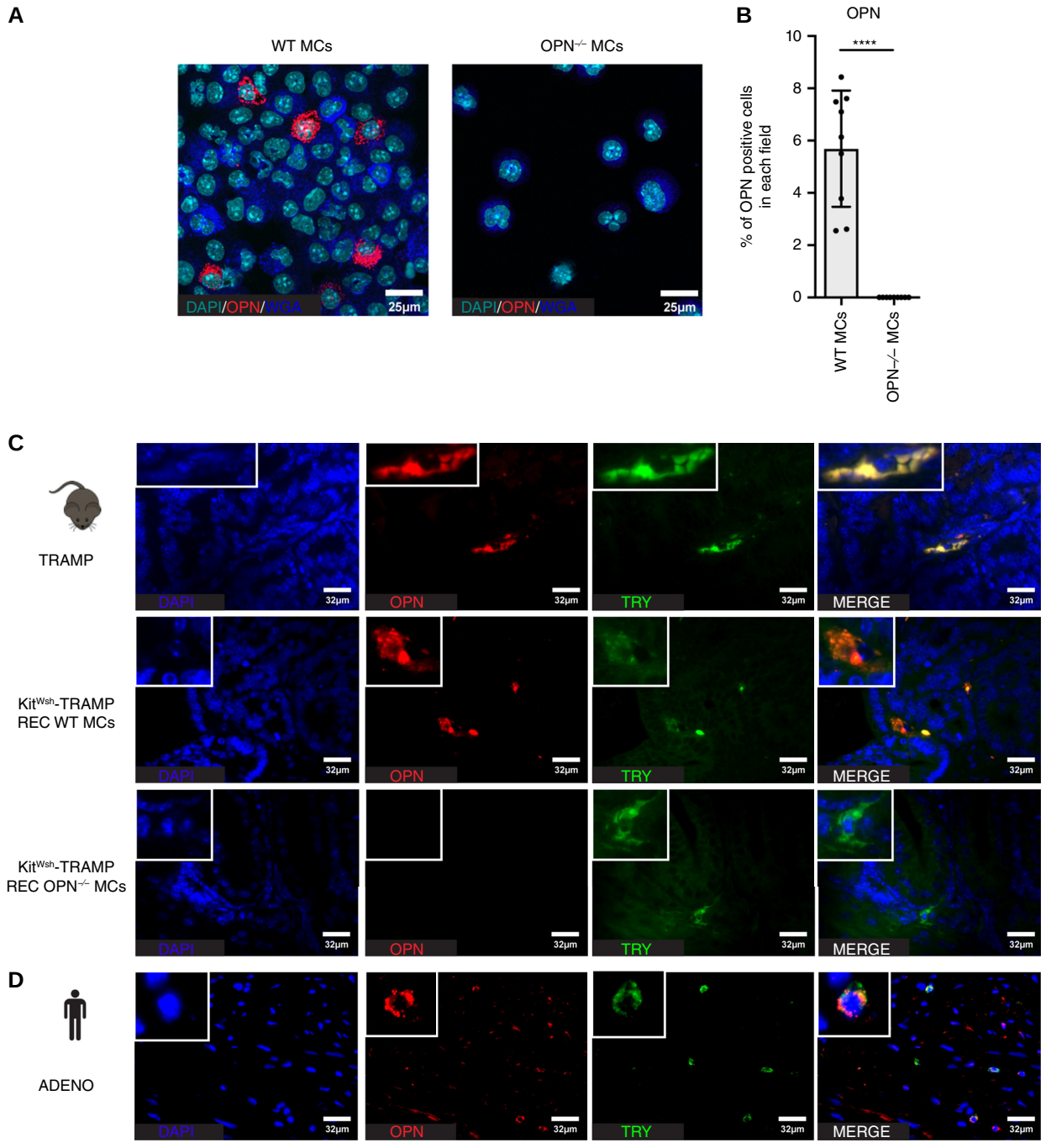

Figure 1.

OPN-proficient MCs are able to restrain NEPC in mice. **A,** Immunofluorescence for DAPI (cyan), WGA (blue), and OPN (red) on WT and OPN$^{-/-}$ MCs. Images were acquired with a confocal microscope. **B,** Quantification of **A** as a percentage of OPN-positive cells in each field. The histogram depicts the mean ± SD of biological replicates (represented by dots; $n = 9$ per group). Unpaired t test was used: ****, $P < 0.0001$. **C,** Representative immunofluorescence for DAPI (blue), OPN (red), and TRY (green) on prostates of a TRAMP mouse and of Kit^{Wsh}-TRAMP mice reconstituted either with WT or OPN$^{-/-}$ MCs. **D,** Representative immunofluorescence for DAPI (blue), OPN (red), and TRY (green) on a human prostate adenocarcinoma sample. (*Continued on the following page.*)

AR^{low}/NE^{-}; DNPC, AR^{-}/NE^{-}; and SNPC, AR^{-}/NE^{+}) were downloaded from the GEO repository (https://www.ncbi.nlm.nih.gov/geo/) at GSE126078. For every sample, the RNA-seq data were downloaded and imported into R software (R Core Team) in which a unique gene expression matrix for every sample was constructed. Then, the gene expression matrix was filtered for all the samples and for our gene of

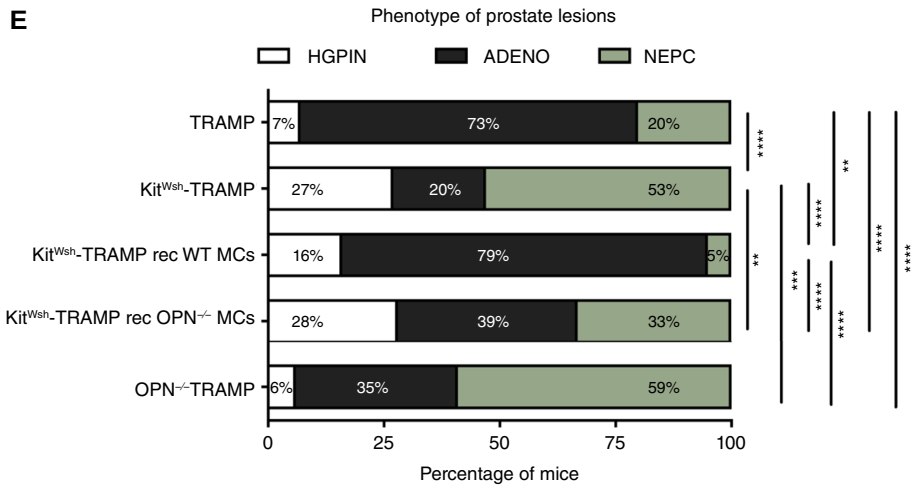

Figure 1.

(*Continued*.) **E,** Percentage of prostate lesions scored as high-grade prostate intraepithelial neoplasia (HGPIN), adenocarcinoma (ADENO), or NEPC in 25–30-week-old TRAMP ($n = 15$), Kit^{Wsh}-TRAMP ($n = 15$), or OPN$^{-/-}$TRAMP mice ($n = 17$). Where indicated Kit^{Wsh}-TRAMP mice were reconstituted i.p. with 5×10^6 WT ($n = 19$) or OPN$^{-/-}$ ($n = 18$) MCs at the age of 8 weeks. Numbers within bars represent the percentage of mice with the indicated histology. Fisher exact test was used for the analysis of contingency between different groups. *P* values are reported as: **, $P < 0.01$; ***, $P < 0.001$; ****, $P < 0.0001$. Where the *P* value is not indicated, the comparison between groups is not statistically significant.

interest (*Sdc1*). Boxplots were performed using R software and analyzed using one-way ANOVA.

To perform the single-cell RNA-sequencing analysis, we utilized the publicly available data published by Han and colleagues obtained from the TPPRC mouse model (30). Cell Ranger ARC 1.0.1 output data was retrieved from the National Genomics Data Center under the accession code OMIX001928. We followed the normalization and filtering methods described by Han and colleagues to ensure the inclusion of low-count cell types, such as immune cells. Following clustering, we identified and excluded cluster 0, which exhibited low-quality cells, as evidenced by a high percentage of mitochondrial genes and a low gene count. Subsequently, we conducted clustering on the cells that passed the filtering criteria, employing the Leiden algorithm with a resolution parameter set to 0.4, resulting in the identification of 20 distinct clusters. To annotate cell types, we evaluated the expression of known marker genes. We identified differentially expressed genes in each cluster using the Wilcoxon rank-sum test; *P* values were then corrected with the Benjamini–Hochberg procedure. In the dotplots, the color of the dot represents the standardized mean expression of the gene in the cluster and the size of the dot indicates the fraction of cells expressing the gene in the cluster.

We also analyzed two data sets generated in the lab from TRAMP mice, comparing the transcriptome of adenocarcinoma with that of full-grown NEPC (data set generated in ref. 6 and available at GEO under the accession number GSE29958) or of incipient NEPC lesions (Clariom S microarray analysis generated in this study; GSE242811). Heatmap representations were performed using R software (R Core Team) and class comparisons with the *limma* R package. The MetaCore software (Clarivate Analytics, Philadelphia) was used for pathway analyses. *P* value was corrected with the Benjamini–Hochberg method; genes were considered significant with FDR <0.05.

Statistical analyses and reproducibility

Statistical analyses were performed with GraphPad Prism9 software (GraphPad Software, La Jolla, CA, USA, RRID: SCR_002798). All *in vitro* experiments were performed at least two times. Pools of all the biological replicates from all the independent experiments were performed and shown in histograms; statistical analysis was run considering all the samples. Histograms report means ± SD of all biological replicates, which are represented by dots. Data were analyzed using One-way ANOVA with *posthoc* Tukey's test for multiple comparisons, or the Wilcoxon Mann–Whitney test, as indicated. For ethical reasons, the number of animals used for *in vivo* studies was the minimum necessary to ensure the significance of the results. The sample size is indicated in figure legends and was defined to obtain an effect size of 0.4 with 80% power and an error of 5% ($a = 0.05$). We used the Fisher test for comparison of categorical variables indicating the phenotype of tumor lesions. In all statistical comparisons, differences were considered significant when $P < 0.05$, and *P* values were reported as follows: *, $P < 0.05$; **, $P < 0.01$; ***, $P < 0.001$; ****, $P < 0.0001$. Where the *P* value is not indicated, the comparison between groups is not statistically significant.

Data availability

The data underlying the gene expression profiles of NEPC and adenocarcinoma samples from TRAMP mice are openly available in the GEO database (GSE242811). All other data generated in the study are available in the manuscript and its supplementary files or from the corresponding author upon reasonable request.

Results

OPN-expressing MCs limit the frequency of NEPC *in vivo*

Our previous work suggested that MCs can restrain the growth of NEPC by producing OPN (6, 8, 9). To test this hypothesis, we first checked OPN expression in primary cultures of MCs obtained *in vitro* from the bone marrow of wild-type C57BL/6 or OPN-deficient mice (hereafter named as WT MCs or OPN$^{-/-}$ MCs, respectively), confirming by immunofluorescence the presence of

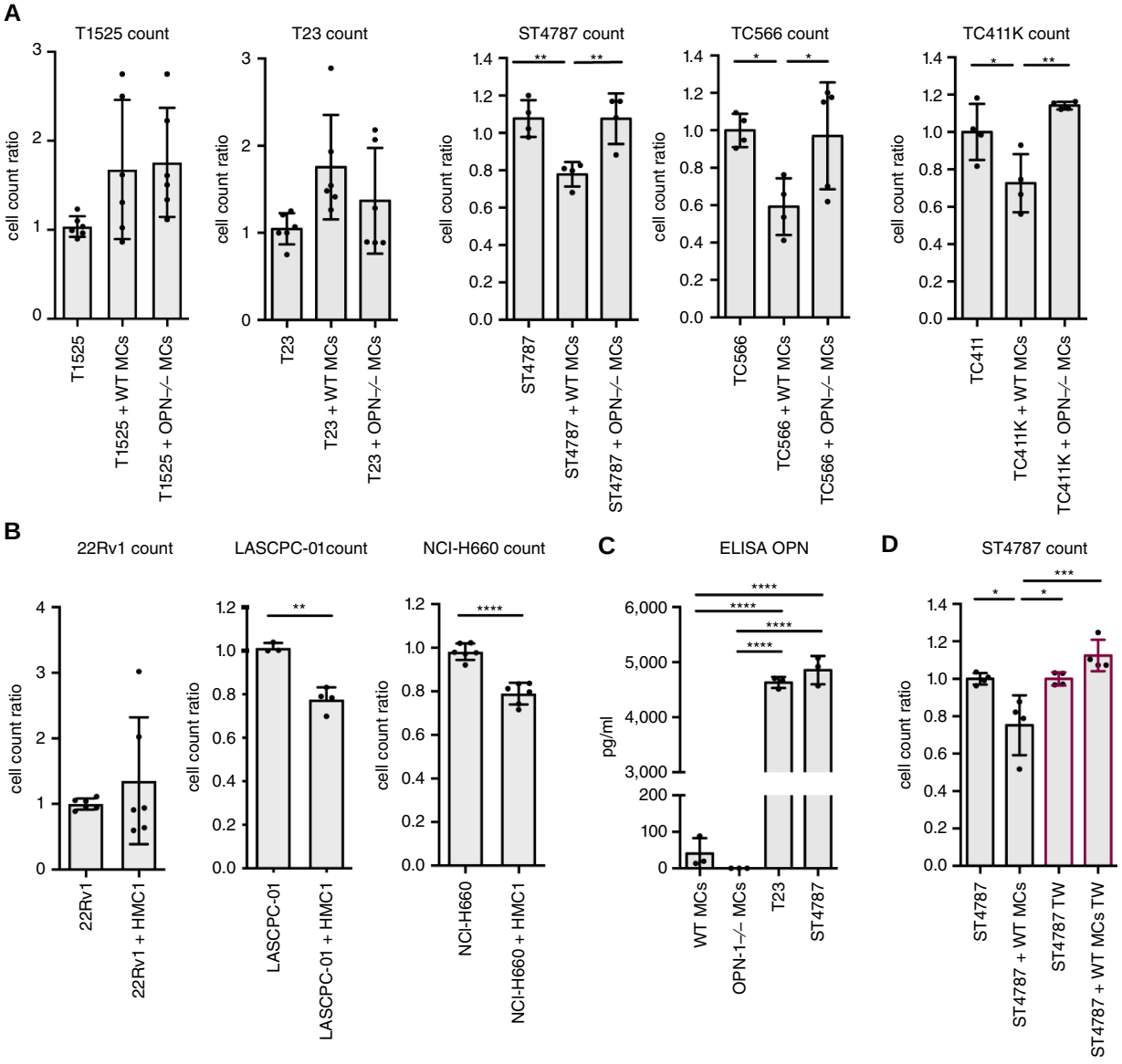

Figure 2.

iOPN mediates the inhibitory function of MCs against NEPC. **A,** Murine adenocarcinoma (T1525 and T23; $n = 6$ per group) and NEPC (ST4787, TC566, and TC411K; $n = 4$ per group) cells (50,000/well) were cultured either alone or with either WT or OPN$^{-/-}$ MCs (tumor cell:MC ratio 1:1). After 4 days the growth rate of cancer cells was evaluated through trypan blue count. Cancer cells and MCs could be distinguished thanks to their growth in adhesion or suspension, respectively. **B,** Human adenocarcinoma (22Rv1; $n = 6$ per group) and NEPC (LASCPC-01, $n = 3$ per group and NCI-H660, $n = 6$ per group) cells (100,000/well), were cultured either alone with the human MC cell line HMC1 for 4 days (tumor cell:MC ratio 1:1). The growth rate of cancer cells was evaluated through flow cytometry. Cancer cells and MCs could be distinguished thanks to the selective expression of CD49f and c-Kit respectively, (gating strategy in Supplementary Fig. S4D). **C,** Secretion of OPN by Supplementary Fig. S4D). **C,** Secretion of OPN by MCs and prostate cancer cells measured by ELISA in culture supernatants ($n = 3$ per group). **D,** Murine ST4787 NEPC cells were cultured either alone or with MCs (tumor cell:MC ratio 1:1; $n = 4$ per group). Where indicated cells were seeded in a 0.4 μmol/L transwell system (TW). Tumor cell growth was evaluated as in **A**. (*Continued on the following page.*)

OPN in the former (**Fig. 1A** and **B**; Supplementary Fig. S2A and S2B). Then, we examined MC infiltration in untreated prostate tumors, finding that, consistent with our previous publications (6–8), MCs highly infiltrated adenocarcinoma, whereas their count dropped in NEPC, both in TRAMP and human tumors (Supplementary Fig. S3A). Therefore, we checked OPN expression *in vivo* in MCs infiltrating prostate adenocarcinoma lesions in TRAMP mice (**Fig. 1C**) and in MC-deficient Kit^{Wsh}-TRAMP mice that were previously reconstituted with either WT or OPN$^{-/-}$ MCs. Both TRAMP mice and Kit^{Wsh}-TRAMP mice reconstituted with WT MCs exhibited a positive staining for OPN in prostate-infiltrating MCs, identified as tryptase (TRY) positive cells (**Fig. 1C**). We also confirmed OPN expression in MCs infiltrating human prostate adenocarcinoma (**Fig. 1D**).

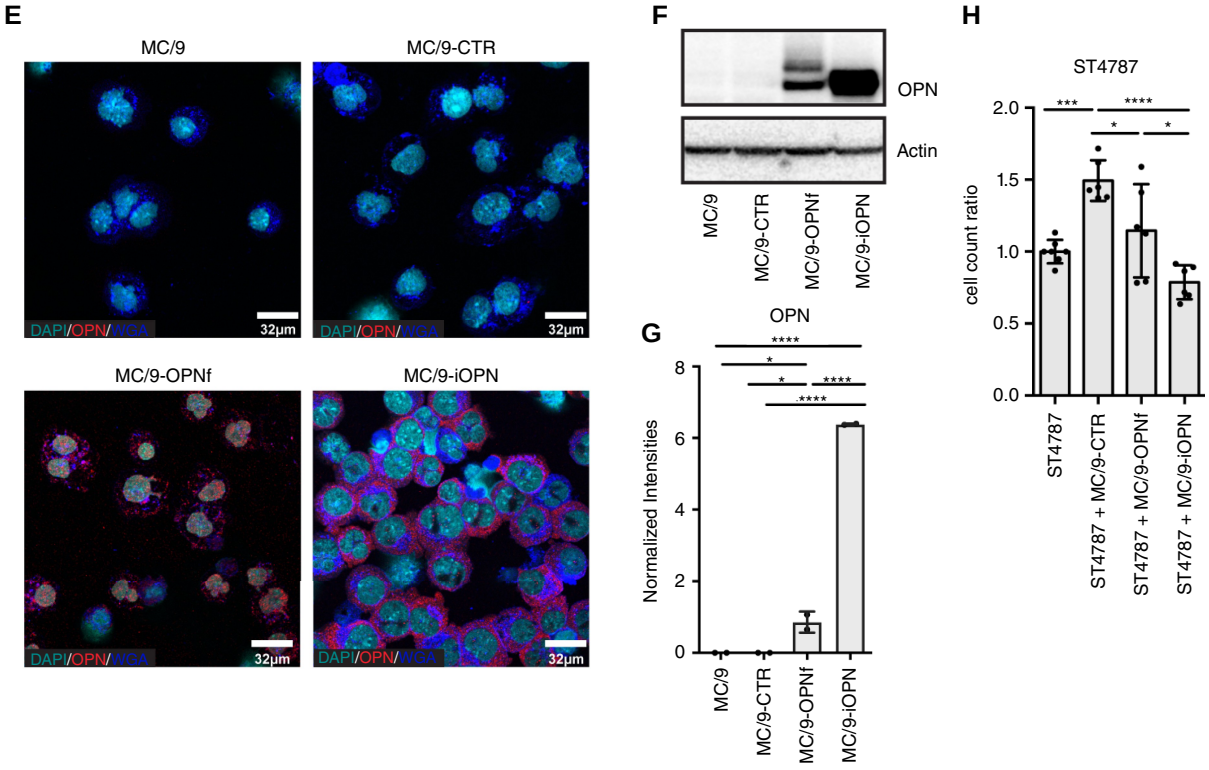

Figure 2.

(*Continued.*) **E,** Immunofluorescence for DAPI (cyan), WGA (blue), and OPN (red) in MC/9, MC/9-CTR, MC9-OPNf, and MC/9-iOPN cells. Images were acquired with a confocal microscope. **F,** Western blot for OPN in cell lysates from MC/9, MC/9-CTR, MC9-OPNf, and MC/9-iOPN cells. The western blot was validated twice. **G,** Quantification of **F** ($n = 2$ per group). **H,** Murine ST4787 NEPC cells were cultured either alone or with MC/9-CTR, MC/9-OPNf, or MC/9-iOPN (tumor cell:MC ratio 1:1; $n = 6$ per group). Tumor cell proliferation was evaluated as in **A** to **D**, **G**, and **H,** All *in vitro* experiments were performed at least two times. Pools of all the biological replicates from all the independent experiments were performed and shown in histograms; statistical analysis was run considering all the samples. All histograms depict mean ± SD of biological replicates (represented by dots). One-way ANOVA followed by Tukey's multiple comparison test was used: *, $P < 0.05$; **, $P < 0.01$; ***, $P < 0.001$; ****, $P < 0.0001$. Where the P value is not indicated, the comparison between groups is not statistically significant.

Then, we compared tumor growth between cohorts of 30-week-old TRAMP, Kit^{Wsh}-TRAMP, OPN$^{-/-}$ TRAMP mice, and Kit^{Wsh}-TRAMP mice reconstituted at 8 weeks of age with WT or OPN$^{-/-}$ MCs (**Fig. 1E**). The i.p. reconstitution procedure allows efficient migration and survival of MCs at the tumor site (6, 7). Indeed, toluidine blue staining confirmed the repopulation of MCs within the prostate lesions, as well as their persistence until 30 weeks of age, in Kit^{Wsh}-TRAMP mice reconstituted with either WT or OPN$^{-/-}$ MCs (Supplementary Fig. S3B). We also verified that MCs were properly infiltrating the prostates of OPN$^{-/-}$TRAMP mice as well (Supplementary Fig. S3B). The majority of TRAMP mice developed prostatic lesions defined as HGPIN (7% of mice) or adenocarcinoma (ADENO, 73% of mice), and only a small percentage (20%) showed evidence of NEPC. Confirming our previous work, histopathological evaluation of prostate lesions showed that the genetic ablation of MCs or OPN significantly raised the frequency of NEPC compared with TRAMP mice (53%, 59%, and 20% of mice, respectively in Kit^{Wsh}-TRAMP, OPN$^{-/-}$TRAMP, and TRAMP mice). The adoptive transfer of WT MCs significantly reduced the frequency of NEPC in Kit^{Wsh}-TRAMP mice, which turned out to be even lower than that of untreated age-matched control TRAMP mice (5% and 20% in Kit^{Wsh}-TRAMP and TRAMP mice, respectively). On the contrary, the adoptive transfer of OPN$^{-/-}$ MCs induced only a slight reduction of NEPC frequency (33% of NEPC), which did not reach the levels found in Kit^{Wsh}-TRAMP mice reconstituted with WT MCs. Indeed, the rate of NEPC was 53% in Kit^{Wsh}-TRAMP mice, and was reduced to 5% and 33% in Kit^{Wsh}-TRAMP mice that received WT or OPN$^{-/-}$ MCs, respectively (**Fig. 1E**). Therefore, WT MCs proved to have a superior ability than OPN$^{-/-}$ MCs in inhibiting NEPC growth in TRAMP mice. These results indicate that OPN mediates at least part of the protective role of MCs against NEPC development *in vivo*.

iOPN restrains the growth of NEPC cells *in vitro* in a cell-cell contact fashion

To dissect the molecular effects of MC-derived OPN on NEPC growth, we evaluated the growth of different TRAMP-derived adenocarcinoma (T1525 and T23; ref. 6) or NEPC cells (ST4787, TC566, and TC411K; ref. 20; Supplementary Fig. S4A), when cultured in the presence of either WT or OPN$^{-/-}$ MCs. We found that, regardless of OPN expression, MCs did not significantly influence the growth of either the T1525 or T23 adenocarcinoma cells (**Fig. 2A**). In contrast, WT MCs, but not OPN$^{-/-}$ MCs, significantly decreased the growth of ST4787, TC566, and TC411K NEPC cells (**Fig. 2A**). We then repeated these experiments with a panel of human adenocarcinoma (22Rv1) and NEPC (LASCPC-01 and NCI-H660) cell lines, co-cultured with the human MC line HMC1 (22), which expresses OPN (Supplementary Fig. S4B and S4C). Also in

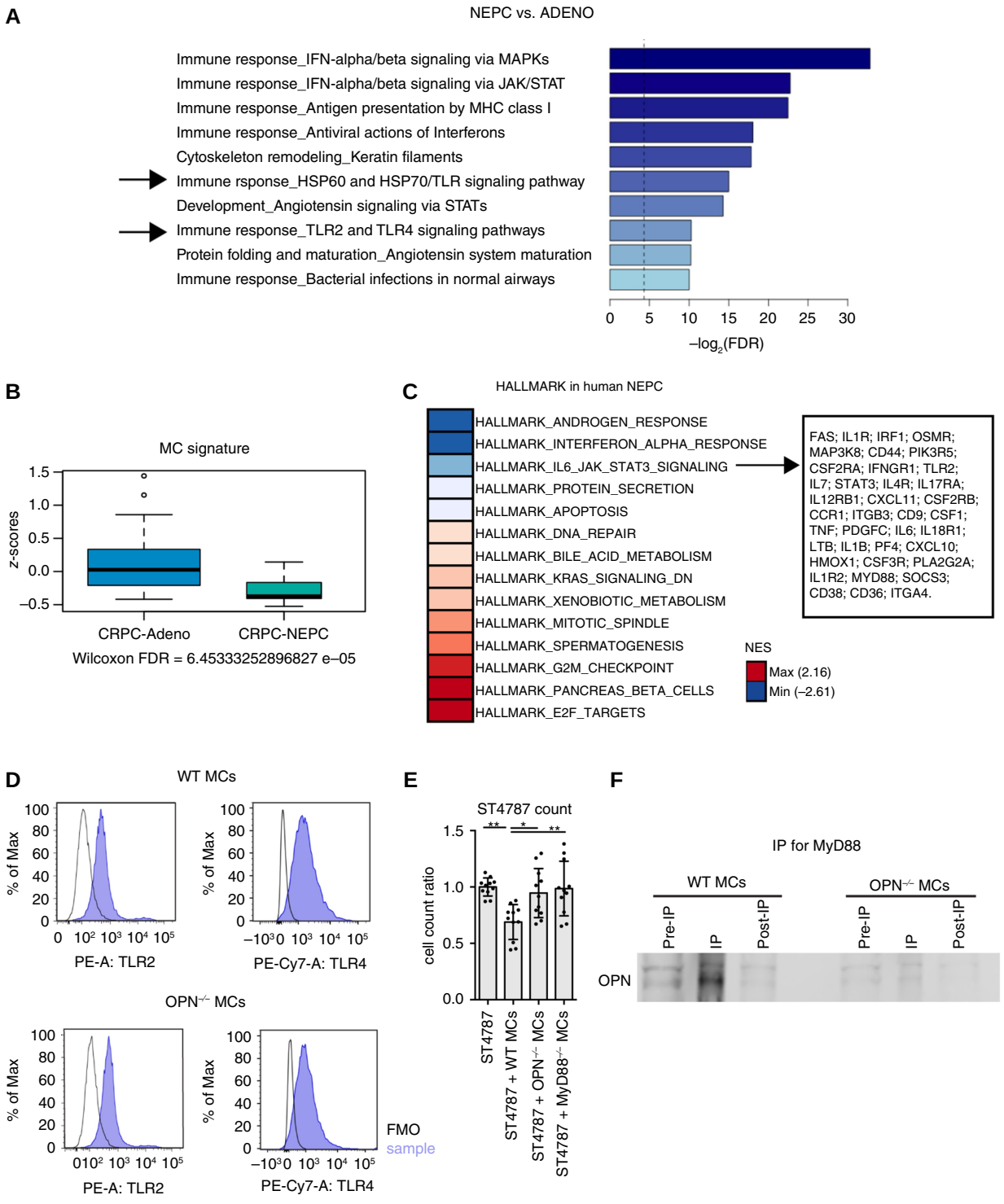

Figure 3.

iOPN regulates the TLR pathway in MCs. **A,** Pathways significantly downregulated in NEPC tumors vs. adenocarcinoma of TRAMP mice (dataset that we generated in ref. 6) identified by the MetaCore software. **B,** RNA-seq normalized data (*z*-scores) of castration-resistant prostate adenocarcinoma (CRPC-Adeno) and NEPC (CRPC-NEPC) samples from the human Beltran Data set (25) were downloaded from c-BioPortal and filtered for the genes composing a MC signature that we previously generated (7). The boxplot represents the mean expression of the MC signature in CRPC-Adeno and CRPC-NEPC. The adjusted *P* value between the two groups was calculated using the Wilcoxon-Mann–Whitney test with Benjamini & Hochberg (FDR) correction. **C,** GSEA performed on the Beltran data set of human CRPC-Adeno and CRPC-NEPC tumor samples. The heatmap shows the significantly enriched upregulated (red) and downregulated (blue) pathways in NEPC, based on normalized enrichment scale. The box specifies the enriched genes in the downregulated (*Continued on the following page.*)

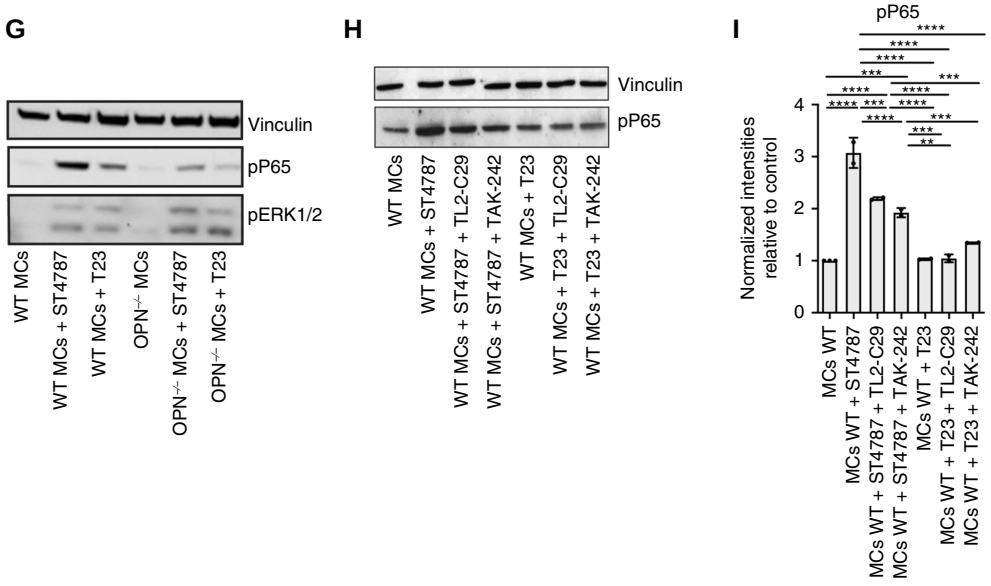

Figure 3.

(*Continued*.) hallmark pathway "IL6_JAK_STAT3_signaling." **D,** Flow cytometry evaluation of TLR2 and TLR4 in WT and OPN$^{-/-}$ MCs. **E,** ST4787 cells (50,000/well) were co-cultured with WT, OPN$^{-/-}$, or MyD88$^{-/-}$ MCs (tumor:MC ratio 1:1; $n = 11$ per group). Tumor cell growth rate was evaluated by trypan blue count. **F,** Immunoprecipitation for MyD88 in WT and OPN$^{-/-}$ MCs after stimulation with LTA (10 μg/mL) and lipopolysaccharide (1 μg/mL) for 30 minutes. Immunoprecipitated samples were then subjected to western blot for OPN. Immunoprecipitation was validated twice. **G,** Western blot for phosphorylated (p)P65 and pERK1/2 evaluation in WT or OPN$^{-/-}$ MCs, either unstimulated or after co-culture with ST4787 or T23 (ratio 1:1) for 15 minutes. The western blot was validated twice. **H,** Western blot for phosphorylated (p) P65 in WT MCs, either unstimulated or co-cultured with ST4787 or T23 cells (ratio 1:1) for 15 minutes. Where indicated, a specific inhibitor of either TLR2 (TL2-C29, 50 μg/mL) or TLR4 (TAK-242, 100 nmol/L) was added. The western blot was validated twice ($n = 2$). **I,** Quantification of **H**. All *in vitro* experiments were performed at least two times. Pools of all the biological replicates from all the independent experiments were performed and shown in histograms; statistical analysis was run considering all the samples. All histograms depict mean ± SD of biological replicates (represented by dots). One-way ANOVA followed by Tukey's multiple comparison test was used for the analysis of significance between samples. *P* values are reported as: *, $P < 0.05$; **, $P < 0.01$; ***, $P < 0.001$; ****, $P < 0.0001$. Where the *P* value is not indicated, the comparison between groups is not statistically significant.

this human setting, we found that OPN-expressing MCs did not affect the growth of 22Rv1 adenocarcinoma cells, but significantly reduced the growth of both LASCPC-01 and NCI-H660 NEPC cells (**Fig. 2B**; Supplementary Fig. S4D).

These data confirmed that MC-derived OPN can reduce NEPC cell growth. As the two translational OPN isoforms, secreted (sOPN) and intracellular (iOPN), can exert different functions (31, 32), we decided to investigate which one was relevant for this MC function. Despite staining positive for OPN (**Fig. 1A**), MCs released a small amount of sOPN compared with tumor cells (**Fig. 2C**). This prompted us to hypothesize a protective role of iOPN expressed by MCs against NEPC. To exclude the role of sOPN in blocking NEPC progression, we repeated the described co-culture experiments segregating the two cell types by a transwell system. The presence of the transwell abrogated the effect of MCs in reducing ST4787 growth (**Fig. 2D**), indicating that contact between MCs and tumor cells was necessary to restrain NEPC cell growth and excluding the involvement of the secreted form of OPN in this function.

To prove the relevance of the intracellular isoform of OPN, we took advantage of the murine immortalized MC cell line MC/9 (21), which does not express endogenous OPN (**Fig. 2E–G**; Supplementary Figs. S4E and S4F and S5A and S5B). We used lentiviruses to overexpress in MC/9 cells either the full-length OPN transcript (OPNf, able to give the production of both sOPN and iOPN) or a shorter transcript encoding only for iOPN. MC/9 cells infected with an empty vector were used as a negative control (CTR). Immunofluorescence to detect iOPN (**Fig. 2E**; Supplementary Fig. S5A) revealed that similar percentages of MC/9-OPNf and MC/9-iOPN cells were positive (Supplementary Fig. S5B), but western blot performed on cell lysates indicated that the levels of iOPN were approximately six times higher in MC/9-iOPN cells compared with MC/9-OPNf cells (**Fig. 2F** and **G**). Furthermore, ELISA showed that MC/9-OPNf cells released high amounts of sOPN in their supernatants (Supplementary Fig. S4F). We also detected a tiny amount of sOPN in the supernatant of MC/9-iOPN cells (Supplementary Fig. S4F). This could be due to the forced overexpression of the protein by the lentiviral expression system that results in a passive release in the extracellular space of an abnormal quantity of OPN. Next, we co-cultured ST4787 NEPC cells with MC/9-CTR, MC/9-OPNf, or MC/9-iOPN to assess their influence on cancer cell growth. MC/9-CTR cells, which do not express endogenous OPN, did not inhibit, but rather fostered, the proliferation of ST4787 cells, likely as a possible side effect of the lentiviral infection (**Fig. 2H**). This differed from WT MCs, which endogenously have OPN (**Fig.1A**; Supplementary Fig. S2A and S2B) and restrained NEPC cell growth (**Fig. 2A**). Yet, the fact that MC/9-CTR cells, devoid of endogenous OPN, did not inhibit NEPC cells reinforced our hypothesis of active involvement of OPN in this function of MCs. Moreover, forcing iOPN expression in MC/9 cells was sufficient to confer on them the ability to significantly suppress the growth of ST4787 NEPC cells, in comparison to the MC/9-CTR co-culture

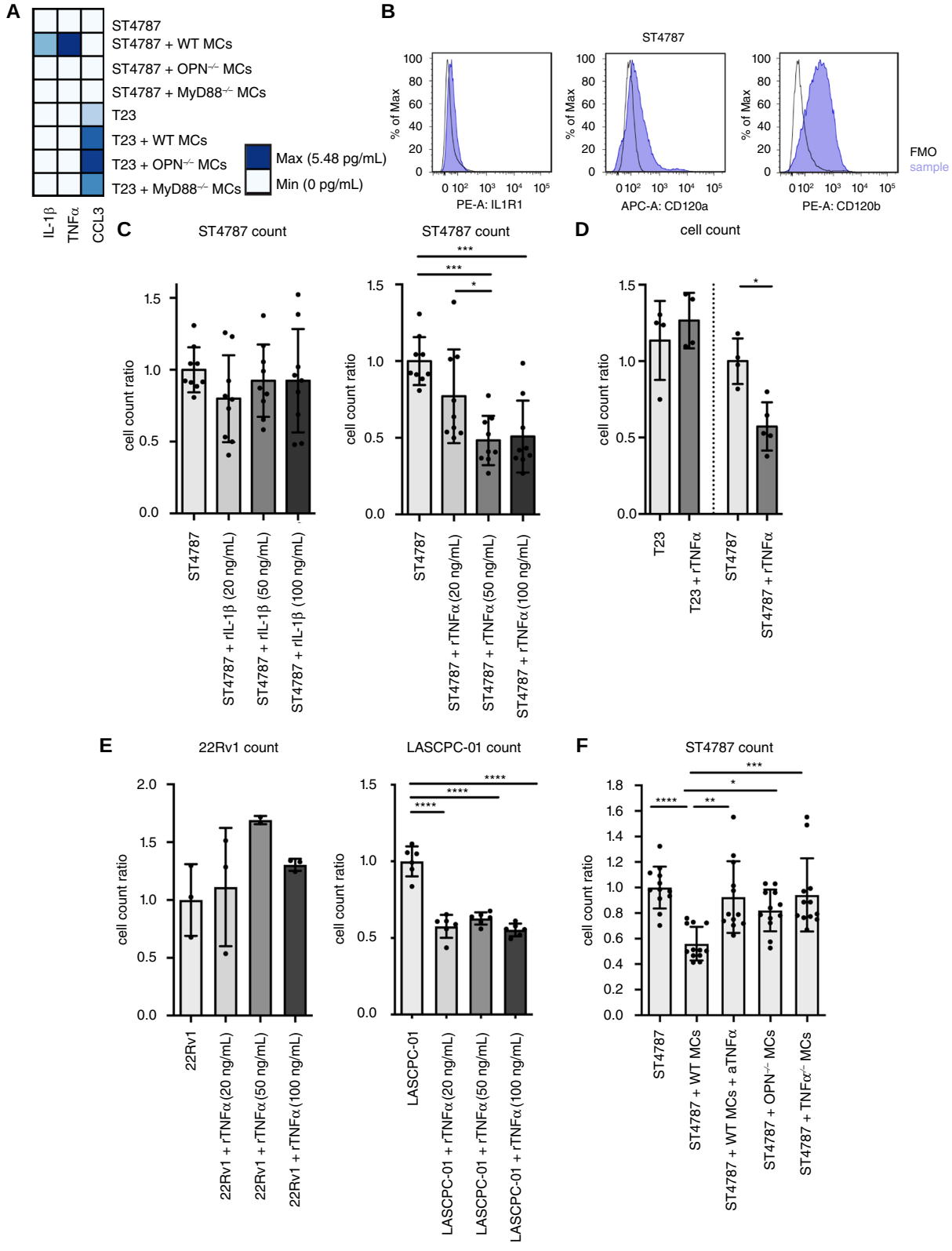

Figure 4.

MC-derived TNFα specifically inhibits the growth of NEPC cells by inducing apoptosis. **A,** Murine NEPC (ST4787) or adenocarcinoma (T23) cells (50,000/well) were cultured either alone or in the presence of WT, OPN$^{-/-}$, or MyD88$^{-/-}$ MCs (tumor cell:MC ratio 1:1; $n = 3$ per group) for 4 days. The heatmap reports (*Continued on the following page.*)

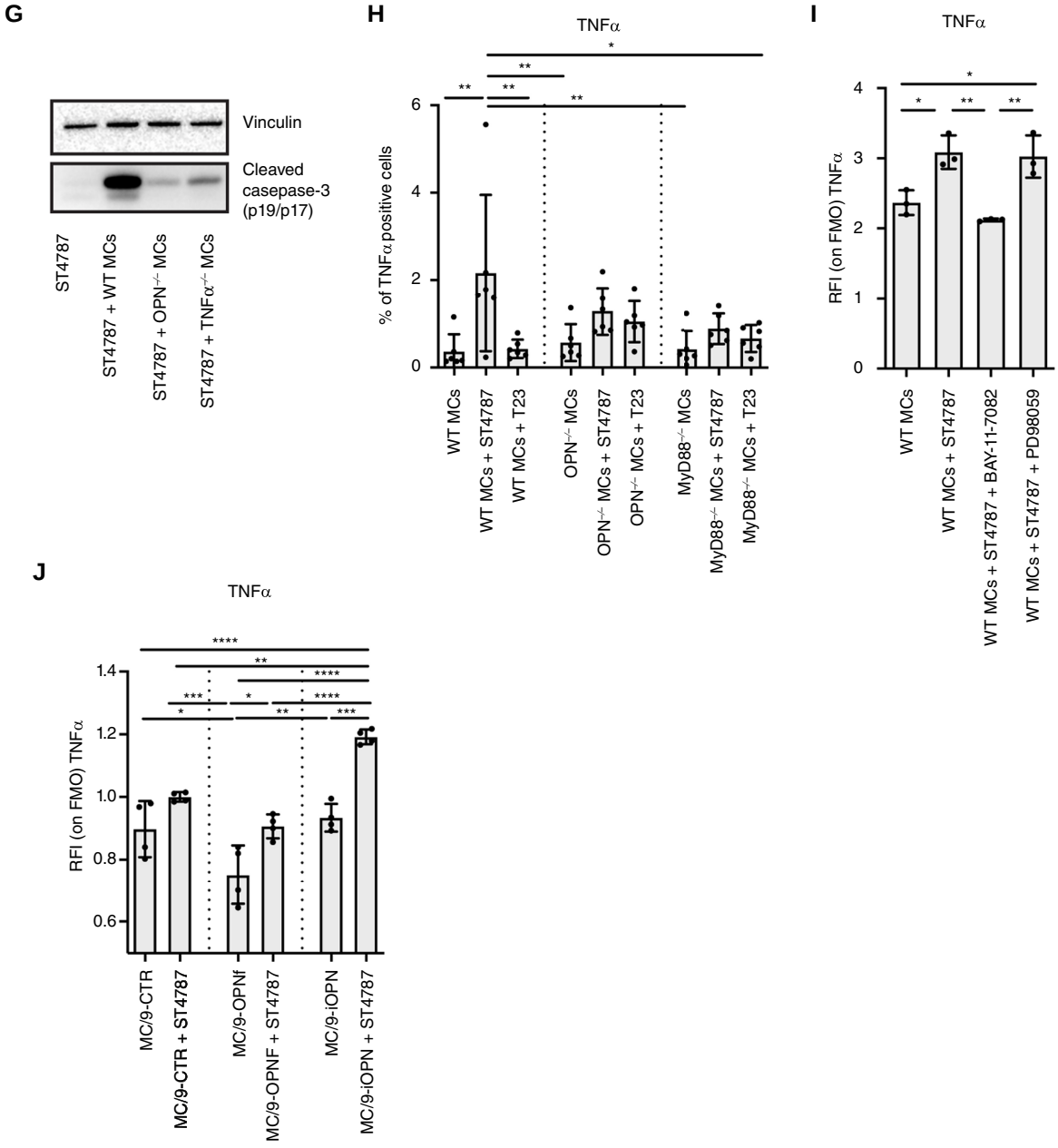

Figure 4.

(*Continued.*) the evaluation of IL1β, TNFα, and CCL3 as measured utilizing a multiple immunoassay kit (ProcartaPlex by Thermo Fisher). **B,** Flow cytometry evaluation of IL1R, and TNFRs (CD120a and CD120b) on ST4787 cells. **C,** ST4787 NEPC cells were treated with different concentrations (20, 50, or 100 ng/mL) of recombinant (r) IL1β or TNFα ($n = 9$ per group). Tumor cell proliferation was evaluated through trypan blue count after 4 days. **D,** T23 (adenocarcinoma) or ST4787 (NEPC) cells were treated with 50 ng/mL of rTNFα and analyzed as in **C** ($n = 4$ per group). **E,** Human adenocarcinoma (22Rv1; $n = 3$ per group) and NEPC (LASCPC-01; $n = 6$ per group) cells were treated with different concentrations (20, 50, or 100 ng/mL) of rTNFα and analyzed as in **C**. **F,** ST4787 cells (50,000/well) were cultured either alone or with WT, OPN$^{-/-}$, or TNFα$^{-/-}$ MCs (tumor cell:MC ratio 1:1). Where indicated, a blocking antibody against TNFα (aTNFα; V1q clone, 10 μg/mL) was added. Tumor cell proliferation was analyzed as in **C**. $N = 9$ per group. **G,** Western blot analysis for cleaved-caspase-3 evaluation in ST4787 cells either unstimulated or co-cultured with WT, OPN$^{-/-}$, or TNFα$^{-/-}$ MCs (ratio 1:1) for 15 minutes. The western blot was validated twice. **H,** Evaluation of TNFα production by intracellular flow cytometry in WT, OPN$^{-/-}$, or MyD88$^{-/-}$ MCs, either unstimulated or cultured for 16 hours with ST787 or T23 cells (MC:tumor cell ratio 1:1; $n = 6$ per group). Gating strategy is reported in Supplementary Fig. S7D. **I,** WT MCs were cultured either alone or in the presence of ST4787 cells (MC:tumor cell ratio 1:1; $n = 3$ per group). Where indicated, an inhibitor of either NF-κB (BAY-11-7082, 10 μmol/L) or ERK1/2 (PD98059, 10 μmol/L; this compound inhibits MEK, which is upstream ERK1/2) pathway was added. After 16 hours, TNFα production by MC/9 was evaluated by flow cytometry as in **H**. Histogram reports the relative fluorescence intensity (RFI; ratio of the mean fluorescence intensity of the stained sample and of the fluorescence minus one control). **J,** MC/9-CTR, MC/9-OPNf, and MC/9-iOPN cells were cultured either alone or with ST4787 cells (MC:tumor cell ratio 1:1; $n = 4$ per group). After 16 hours, TNFα production by MC/9 was evaluated by flow cytometry as in **H**. Histogram reports the RFI (ratio of the mean fluorescence intensity of the stained sample and of the fluorescence minus one control), normalized to control condition (MC/9-CTR+ST4787 cells). **C** to **F** and **H** to **J,** All *in vitro* experiments were performed at least two times. Pools of all the biological replicates from all the independent experiments were performed and shown in histograms; statistical analysis was run considering all the samples. All histograms depict mean ± SD of biological replicates (represented by dots). One-way ANOVA followed by Tukey's multiple comparison test (**C**, **E**, **F**, **H**, **I**, and **J**) or Mann–Whitney test (**D**) was used for the analysis of significance between samples. *P* values are reported as: *, $P < 0.05$; **, $P < 0.01$; ***, $P < 0.001$; ****, $P < 0.0001$. Where the *P* value is not indicated, the comparison between groups is not statistically significant.

condition (**Fig. 2H**). The proliferation of tumor cells in the ST4787+MC/9-iOPN condition was consistently but not significantly reduced if compared with ST4787 alone (**Fig. 2H**). MC/9-OPNf cells partially reduced ST4787 growth when compared with MC/9-CTR. This was not surprising to us as OPNf can lead the production of both sOPN and iOPN. The same experiment performed co-culturing MC/9 cells with T23 adenocarcinoma cells showed a trend of increased proliferation of T23 cells after co-culture, regardless of their contact with MC/9-CTR, MC/9-OPNf, or MC/9-iOPN (Supplementary Fig. S5C). These results indicated that restoring iOPN expression in MC/9 cells enabled them to specifically inhibit the growth of NEPC cells. These data prompted us to exclude sOPN and enforced the hypothesis of a protective role of MC-derived iOPN against NEPC.

iOPN mediates the TLR/MyD88 signaling pathway in MCs to restrain NEPC growth

We then investigated the mechanism by which MC-produced iOPN restrains NEPC growth, knowing that iOPN is an adaptor protein binding to MyD88, which can positively or negatively control the activation of signaling pathways downstream of TLR2, TLR4, and TLR9, and the consequent secretion of cytokines (13–15, 33). TLR2 and TLR4 are expressed on the cell membrane, whereas TLR9 is located within the cell (34). As we demonstrated the need for MCs to be in contact with NEPC cells to inhibit their growth, our focus was directed toward TLR2 and TLR4, and we did not consider analyzing TLR9, as it can be activated solely by soluble factors, mainly CpG DNA motifs. To interrogate gene expression profiles that we generated from adenocarcinoma or NEPC occurring in TRAMP mice (6), we performed a GSEA, which showed that TLR2/TLR4 signaling pathways were significantly downregulated in NEPC tumors compared with adenocarcinoma (**Fig. 3A**). We then analyzed a human data set that included patients with CRPC or NEPC (25), and we found that an in-house generated MC gene signature (7) was downregulated in NEPC (**Fig. 3B**). Furthermore, by applying GSEA to the same data set, we found that the hallmark pathway "IL6_JAK_STAT3_signaling," which includes genes like *Tlr2* and *Myd88* was significantly downregulated in human NEPC (**Fig. 3C**).

These results showing the anti-correlation of MCs and the TLR2/TLR4 pathways in NEPC strongly reinforced the hypothesis that MCs could restrain NEPC growth via TLR/MyD88/iOPN-mediated functions. It has been described that MCs can express TLRs on their surface (35); consistent with this, we found that BMMCs expressed high levels of both TLR2 and TLR4 (**Fig. 3D**). Furthermore, in a new set of *in vitro* co-culture experiments we showed that, like $OPN^{-/-}$ MCs, MCs generated from the bone marrow of $MyD88^{-/-}$ mice ($MyD88^{-/-}$ MCs) did not block ST4787 NEPC cell growth (**Fig. 3E**). By immunoprecipitation we also demonstrated that iOPN and MyD88 interact in MCs (**Fig. 3F**). We finally corroborated our hypothesis by testing by western blot analyses the activation of the two main signal transduction pathways activated downstream of TLR2/TLR4, namely, the NF-κB and the ERK1/2 MAPK pathways. Results showed that the levels of phosphorylated P65, which we tested as a readout for NF-κB activation, were specifically increased in WT MCs after co-culture with ST4787 NEPC cells, at levels more than triple compared with those in WT MCs cultured with T23 adenocarcinoma cells. This effect was lost in $OPN^{-/-}$ MCs (**Fig. 3G**; Supplementary Fig. S6). Conversely, we found that the phosphorylation of ERK1/2 was triggered at comparable levels in both WT and $OPN^{-/-}$ MCs after co-culture with either NEPC or adenocarcinoma cells (**Fig. 3G**; Supplementary Fig. S6). Furthermore, as NF-κB signaling can be elicited by both TLR2 and TLR4 stimulation, we performed a western blot for phosphorylated P65 in MCs co-cultured with ST4787 cells in the presence of a specific inhibitor for either TLR2 (TL2-C29) or TLR4 (TAK-242). Results showed that both TL2-C29 and TAK-242 reduced the levels of phosphorylated P65, albeit the latter with a stronger effect (**Fig. 3H** and **I**). Therefore, these data suggest that the encounter with NEPC cells stimulates the activation of both TLR2 and TLR4 downstream pathways in WT MCs.

iOPN controls the release of TNFα by MCs to restrain NEPC growth *in vitro*

The data so far suggest that upon encountering NEPC cells, iOPN-expressing MCs are prompted to activate the TLR2/TLR4-MyD88 signaling pathway leading to the release of cytokine(s) that in turn affect tumor growth. The absence of OPN or MyD88 in MCs could alter cytokine release and therefore explain the failure of $OPN^{-/-}$ and $MyD88^{-/-}$ MCs in blocking NEPC cell proliferation. To investigate this hypothesis, we performed a multiplex immunoassay to analyze the secretion of a panel of cytokines/chemokines produced as a consequence of TLR2/TLR4 activation (Supplementary Fig. S7A) in supernatants harvested from NEPC (ST4787) or adenocarcinoma (T23) cells cultured either alone or with WT, $OPN^{-/-}$ or $MyD88^{-/-}$ MCs. We found that IL1β and TNFα were highly produced in the co-culture between ST4787 cells and WT MCs, but not when ST4787 were cultured either alone or in the presence of $OPN^{-/-}$ or $MyD88^{-/-}$ MCs (**Fig. 4A**). These cytokines were not detected when MCs were cultured with T23 cells, suggesting that their production by WT MCs could be specifically triggered by NEPC cells (**Fig. 4A**). T23 cells stimulated different pathways in MCs, as we could specifically detect CCL3 in T23-MC co-cultures, regardless of whether MCs were sufficient or deficient for MyD88 or OPN (**Fig. 4A**).

Given these results, we therefore supposed that TNFα and IL1β might have an antiproliferative role against NEPC. However, we found that ST4787 NEPC cells were negative for IL1R1 receptor, although they expressed both CD120a (TNFR1) and CD120b (TNFR2) on their surface (**Fig. 4B**). Accordingly, recombinant TNFα, but not recombinant IL1β, was able to suppress the growth of ST4787 cells, in a dose-dependent fashion (**Fig. 4C**). Moreover, the same amount of rTNFα did not reduce the growth of T23 adenocarcinoma cells (**Fig. 4D**), even through these cells express TNFα receptors (Supplementary Fig. S7B). To further demonstrate that TNFα specifically inhibits the growth of NEPC but not of prostate adenocarcinoma, we repeated these experiments with the human LASCPC-01 NEPC cell line, which we showed expresses the CD120b receptor (Supplementary Fig. S7C), and the 22Rv1 adenocarcinoma cell line, which was negative for both CD120a and CD120b (Supplementary Fig. S7C). The results showed that recombinant TNFα significantly inhibited the growth of LASCPC-01 NEPC cells (**Fig. 4E**), and did not affect the proliferation of 22Rv1 adenocarcinoma cells.

Results indicated that TNFα is produced in the cultures between WT MCs and NEPC cells and that recombinant TNFα can specifically affect NEPC growth. To prove that MCs are the actual source of TNFα in our setting, we utilized $TNFα^{-/-}$ MCs for co-culture experiments with tumor cells. In contrast to WT MCs, but similar to $OPN^{-/-}$ MCs, $TNFα^{-/-}$ MCs did not hamper the growth of ST4787 NEPC cells (**Fig. 4F**) nor did induce the

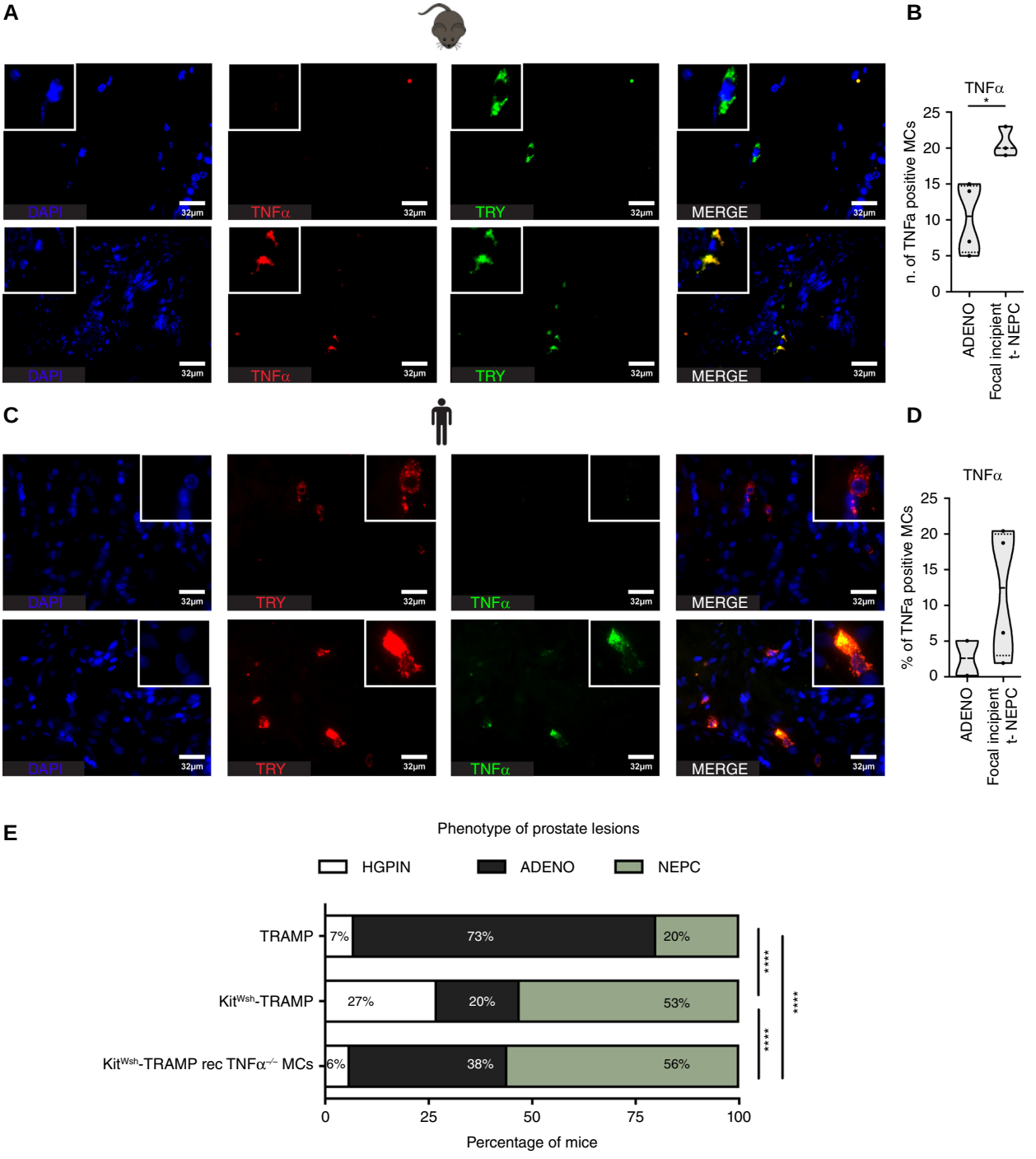

Figure 5.

MC-infiltrating prostates of TRAMP mice and human patients with focal incipient t-NEPC area express TNFα. **A,** Representative immunofluorescence for DAPI (blue), TNFα (red), and TRY (green) on tumor lesions from TRAMP mice subjected to surgical castration, showing either a TNFα-negative (top row) or a TNFα-positive MC (bottom row). **B,** Quantification of TNFα positive MCs in tumor samples from castrated TRAMP mice stained as in **A** ($n = 4$ ADENO and $n = 3$ focal NEPC). **C,** Representative immunofluorescence for DAPI (blue), TRY (red), and TNFα (green) on tumor samples collected from patients who received neoadjuvant ADT, showing either a TNFα-negative or a TNFα-positive MC. **D,** Quantification of TNFα positive MCs in human tumor samples, pretreated with neoadjuvant ADT, stained as in **C** ($n = 2$ ADENO and $n = 4$ focal NEPC). In **B** and **D**, the violin plots depict the median ± SD of biological replicates (represented by dots). Unpaired *t* test was used for statistical analysis: *, $P < 0.05$. Where the *P* value is not indicated, the comparison between groups is not statistically significant. **E,** Percentage of prostate lesions, scored as HGPIN, adenocarcinoma (ADENO), or NEPC in 25–30-week-old Kit^{Wsh}-TRAMP mice reconstituted i.p. with 5×10^6 $TNFα^{-/-}$ MCs ($n = 16$) at the age of 8 weeks. Control cohorts of TRAMP ($n = 15$) and Kit^{Wsh}- TRAMP ($n = 15$) mice are the same as shown in **Fig. 1E**. Numbers within bars represent the percentage of mice with the indicated histology. Fisher exact test was used for the analysis of contingency between different groups. *P* values are reported as: *, $P < 0.05$; **, $P < 0.01$; **, $P < 0.001$; ****, $P < 0.0001$.

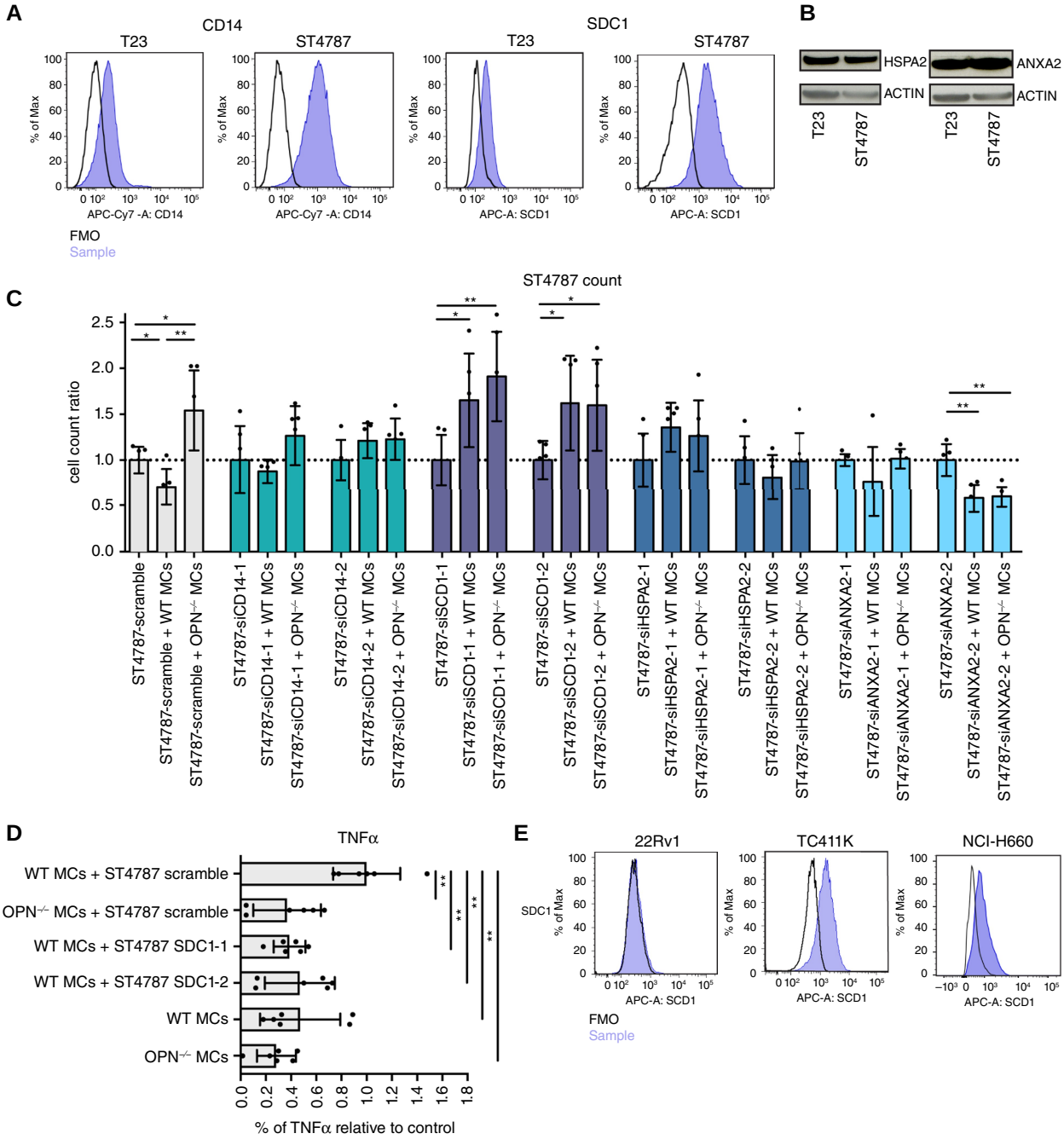

Figure 6.

SDC1 is the NEPC cell-specific ligand that stimulates TNFα secretion by MCs. **A,** Flow cytometry evaluation of CD14 and SDC1 in T23 (adenocarcinoma) and ST4787 (NEPC) cells. **B,** HSPA2 and ANXA2 evaluation by western blot in T23 and ST4787 cells. **C,** ST4787 were silenced with two different siRNA specific for *Cd14* (ST4787-siCD14-1 and ST4787-siCD14-2), *Sdc1* (ST4787-siSDC1-1 and ST4787-siSDC1-2), *Hspa2* (ST4787-siHSPA2-1 and ST4787-siHSPA2-2), *Anxa2* (ST4787-siANXA2-1 and ST4787-siANXA2-2), or for a scramble control (ST4787-scramble). After 72 hours of transfection, ST4787 scramble or silenced cells were cultured either alone or with WT or $OPN^{-/-}$ MCs (tumor cell:MC ratio 1:1; $n = 6$ per group). The growth rate of cancer cells was evaluated through trypan blue count. Cancer cells and MCs could be distinguished, thanks to their growth in adhesion or suspension, respectively. **D,** ST4787 scramble or silenced cells were cultured with WT or $OPN^{-/-}$ MCs (ratio 1:1; $n = 5$ per group). After 16 hours the percentage of TNFα positive MCs was evaluated by flow cytometry, as in **Fig. 4H**. All *in vitro* experiments were performed at least two times. Pools of all the biological replicates from all the independent experiments were performed and shown in histograms; statistical analysis was run considering all the samples. All histograms depict mean ± SD of biological replicates (represented by dots). One-way ANOVA followed by Tukey's multiple comparison test (**D**) or Mann–Whitney test (**C**) was used for the analysis of significance between samples. *P* values are reported as: *, $P < 0.05$; **, $P < 0.01$; ***, $P < 0.001$. Where the *P* value is not indicated, the comparison between groups is not statistically significant. **E,** Flow cytometry evaluation of SDC1 in adenocarcinoma (22Rv1 human) and NEPC (TC411K murine, NCI-H660 human) cells. **F,** (*Continued on the following page.*)

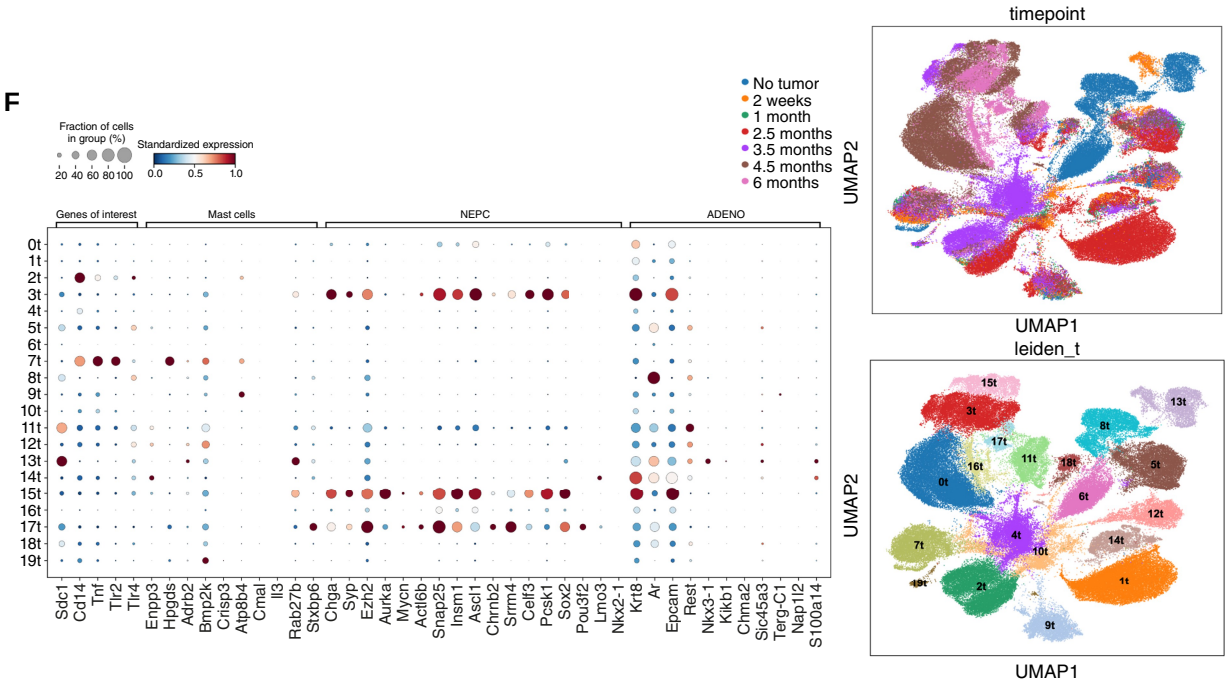

Figure 6.
(*Continued.*) Analyses on the s.c. RNA seq data set of the TPPRC mouse NEPC model (30). Interrogating the data set, we retrieved 20 different clusters of cells. The dot plot graph shows the expression of genes associated with adenocarcinoma, NEPC, MCs, and other genes of interest (*Sdc1*, *Cd14*, *TNfa*, *Tlr2*, and *Tlr4*). Dot size indicates the percentage of cells expressing the gene and dot color indicates the level of gene expression. The UMAPs show the distribution of cells across time of tumor development (top UMAP) and the distribution of the 20 different clusters (bottom UMAP).

cleavage of caspase-3 in ST4787 cells (**Fig. 4G**), which we measured as a readout for TNF-mediated apoptotic cell death (36). Furthermore, adding a TNFα-specific neutralizing antibody in the co-culture of ST4787 cells and WT MCs, the growth rate of NEPC cells was restored (**Fig. 4F**). To further confirm that the TNFα found in the co-cultures (**Fig. 4A**) was exclusively produced by MCs, we relied on flow cytometry, which allowed us to distinguish ST4787 and MC populations thanks to the selective expression of CD49f and CD45, respectively (Supplementary Fig. S7D). We confirmed that contact with NEPC cells specifically triggered TNFα production in MCs, and only if MCs were competent for OPN or MyD88 (**Fig. 4H**). We also repeated this experiment by co-culturing WT MCs with ST4787 cells and adding a specific inhibitor for either NF-κB (BAY-11-7082) or ERK1/2 (PD98059). Results showed that only specific inhibition of NF-κB blunted TNFα production (**Fig. 4I**), therefore pointing to a specific involvement of NF-κB in the TLR/iOPN signaling pathway that leads to TNFα production in MCs after contact with NEPC cells.

Finally, we wanted to determine if iOPN is sufficient to trigger MCs to release TNFα after contact with NEPC cells. Therefore, we evaluated by flow cytometry the production of TNFα by MC/9-CTR, MC/9-OPNf, or MC/9-iOPN, either alone or co-cultured with ST4787 NEPC cells (**Fig. 4J**). Consistent with our hypothesis, the highest levels of TNFα were detected in MC/9-iOPN cells stimulated with ST4787 cells, although we did see some background TNFα production in all the conditions. These results indicated that restoring iOPN in MC/9 cells was sufficient to confer on them the ability to upregulate the production of TNFα after encountering ST4787 cells (**Fig. 4J**).

TNFα is expressed by MCs infiltrating murine and human NEPC and restrains NEPC *in vivo*

Results collected thus far *in vitro* indicated that the TLR/MyD88/iOPN axis plays a crucial role in controlling MC release of TNFα upon specific encounter with NEPC cells, thereby restraining their growth. Nevertheless, our findings also indicated that MCs are absent (**Fig. 3B**; ref. 8) and that TNFα is downregulated in fully developed NEPC (**Fig. 3C**) in patients.

Thus, we hypothesized that, *in vivo*, MCs are still present during the initial phases of NEPC development, when they start to produce TNFα in an effort to control NEPC outgrowth. To prove this hypothesis, we modeled a setting of incipient NEPC in TRAMP mice subjected to surgical castration, a condition that, as we have previously described (23), mimics ADT and induces the emergence of focal NEPC areas within adenocarcinoma (see Supplementary Fig. S8 for H&E staining of representative adenocarcinoma and focal NEPC lesions in prostates from TRAMP mice). Immunofluorescence showed the presence of TNFα-expressing MCs in TRAMP tumors (**Fig. 5A**, showing representative images of prostate lesions with TNFα-negative and TNFα-positive MCs). The number of TNFα-positive MCs was significantly higher in tumors displaying focal NEPC areas, when compared with mice bearing solely adenocarcinoma lesions (**Fig. 5B**). To increase the translational relevance of these results, we retrieved prostatectomies of six patients who had undergone neoadjuvant ADT. We had characterized the histopathologic features of these tumors in a previous publication (23), showing the presence of incipient NEPC areas in four of these samples, whereas the others had only adenocarcinoma lesions (23).

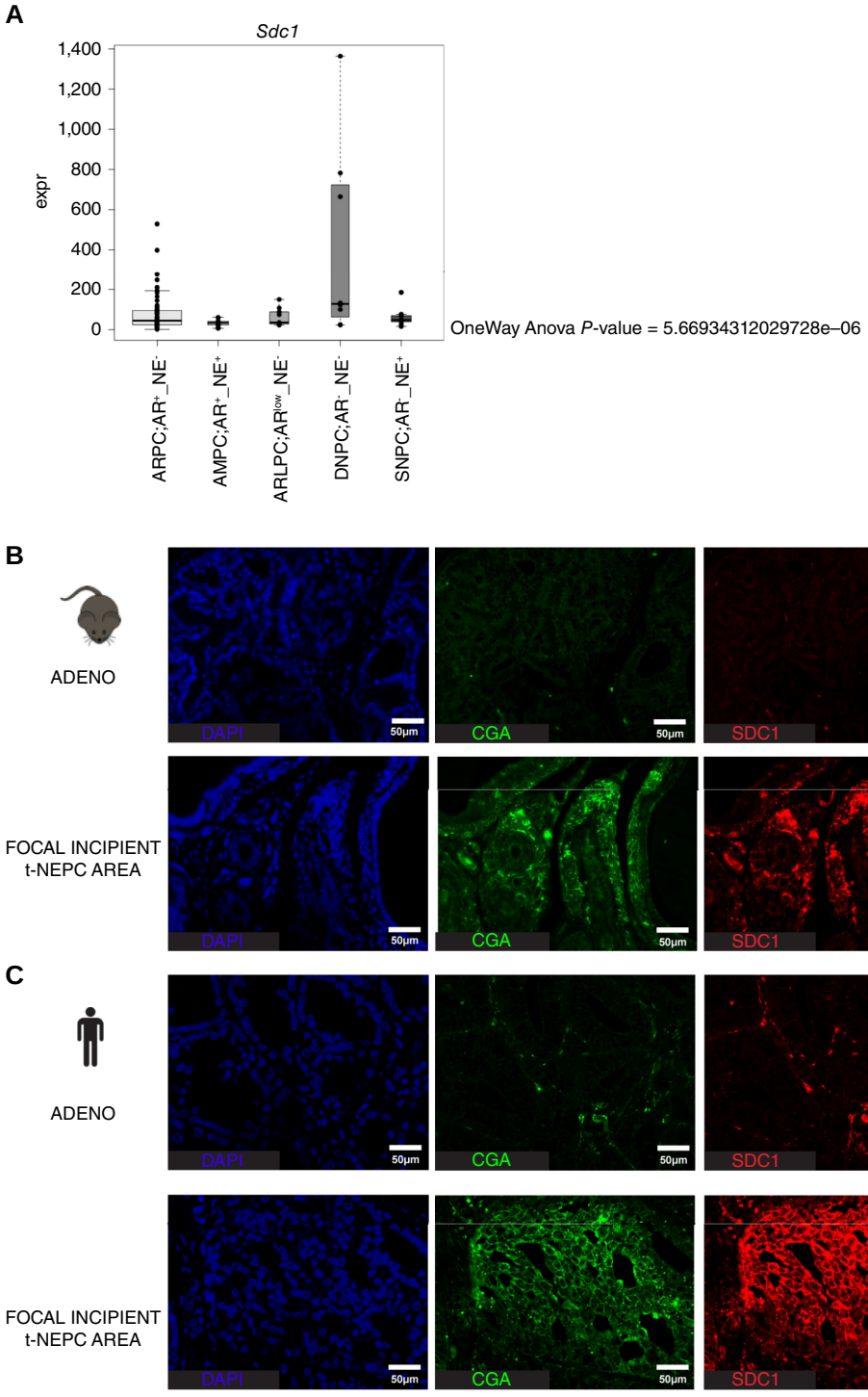

Figure 7.

SDC1 expression levels are low in adenocarcinoma and increase in t-NEPC incipient areas in both murine and human prostates. **A,** Boxplots showing *Sdc1* expression in the five phenotypic groups (ARPC, AR^{+}/NE^{-}; AMPC, AR^{+}/NE^{+}; ARLPC, AR^{low}/NE^{-}; DNPC, AR^{-}/NE^{-}; and SNPC, AR^{-}/NE^{+}) derived from the RNA-seq data of the Labrecque human prostate cancer dataset (29). The RNA-seq data and the metadata containing the association between the samples and the phenotypic groups were downloaded from the GEO repository and the gene expression matrix was filtered for the 98 samples and for our gene of interest (*Sdc1*). The adjusted *P* value between the groups was calculated using the One-way ANOVA. **B,** Immunofluorescence for DAPI (blue), CGA (green), and SDC1 (red) in adenocarcinoma (ADENO) and in focal t-NEPC areas of TRAMP mice, either untreated or subjected to surgical castration, respectively. **C,** Immunofluorescence for DAPI (blue), CGA (green), and SDC1 (red) in adenocarcinoma (ADENO) and in focal t-NEPC areas from patients either untreated or who received neoadjuvant ADT, respectively.

As observed in mice, even in these patient specimens, immunofluorescence (**Fig. 5C**, showing representative images of a TNFα-negative and a TNFα-positive MC in human prostates) revealed a trend of increased accumulation of TNFα-expressing MCs in tumors with focal NEPC areas (**Fig. 5D**). This last result however should be confirmed in a large patient cohort in future studies.

Besides finding a significant increase of TNFα-positive MCs in tumors characterized by incipient NEPC lesions, immunofluorescence analyses identified some scattered TNFα-positive MCs also in adenocarcinoma samples, both in mice and in patients. This might be attributed to the potential interaction of MCs with TLR ligands expressed by other stromal cells within the tumor microenvironment, and not by NEPC cells. Nevertheless, these data underscored that MCs secreting TNFα specifically accumulate in emerging NEPC tumors (**Fig. 5B** and **D**).

To finally prove the protective role of MC-derived TNFα against NEPC *in vivo*, we reconstituted 8-week-old Kit^{Wsh}-TRAMP mice with $TNFα^{-/-}$ MCs, and we sacrificed them at 25 to 30 weeks of age for histopathological evaluation. The persistence of $TNFα^{-/-}$ MCs in the collected tumor lesions was verified by toluidine blue staining (Supplementary Fig. S3B). In this cohort of mice, the frequency of NEPC was comparable to that observed in untreated, MC-deficient, Kit^{Wsh}-TRAMP mice, thus confirming *in vivo* that MCs can inhibit the growth of NEPC by producing TNFα (**Fig. 5E**).

SDC1 on NEPC triggers MC release of TNFα

Finally, we sought to discover which NEPC-derived stimulus activates the TLR2/TLR4 pathway in MCs, promoting the release of TNFα. To this aim, we compared the transcriptomes of TRAMP-derived adenocarcinoma and incipient NEPC lesions, in order to find which genes were upregulated in the latter (List 1, Supplementary Table S3; Supplementary Fig. S9A). Then, interrogating a ligand–receptor pairs repository (LewisLabUCSD; ref. 37), we generated a list of cell-surface ligands for TLR2 and/or TLR4, conserved between mice and humans (List 2, Supplementary Table S3; Supplementary Fig. S9A). The 29 genes shared between List 1 and List 2 represented the final list of possible NEPC-specific surface ligands for TLR2/TLR4 (List 3, Supplementary Table S3; Supplementary Fig. S9A).

We measured transcript levels of these putative ligands in our cell lines by a high-throughput customized Taqman assay, which showed that four out of the 29 genes were upregulated in ST4787 NEPC cells compared with T23 adenocarcinoma cells (Supplementary Table S4). We then further validated the upregulation of these molecules (namely, CD14, SDC1, HSPA2, and ANXA2) in ST4787 NEPC cells by real-time PCR (Supplementary Fig. S9B), flow cytometry (**Fig. 6A**), and western blot (**Fig. 6B**; Supplementary Fig. S9C).

To understand which of these four molecules was able to trigger the production of TNFα in MCs, and consequently inhibit the growth of NEPC cells, we individually silenced each of them in ST4787 cells with two different siRNA (Supplementary Fig. S9D–F), before co-culture with MCs. The silencing of either the *Sdc1* (encoding for the Syndecan-1 protein) or the *Cd14* transcript abolished the suppressive activity of WT MCs against ST4787 cell growth, with consistent results among the two different siRNA used (**Fig. 6C**). Moreover, ST4787 cells silenced for SDC1 proliferated even more in the presence of MCs, regardless of whether they had OPN or not (**Fig. 6C**). This is probably due to an off-target side effect of the siRNA or of the silencing procedure. In contrast, the silencing of other ligands showed no, partial effect, or even contrasting results between the two different sequences of siRNA used (**Fig. 6C**). Silencing of either SDC1 or CD14 in ST4787 cells was also sufficient to abolish their ability to stimulate TNFα production by MCs upon co-culture (**Fig. 6D**; Supplementary Fig. S9G).

These results suggested a potential relevance of both NEPC-expressed SDC1 and CD14 in the cross-talk with MCs. To verify the applicability of this hypothesis across various NEPC models, we evaluated the presence of the two molecules in additional murine and NEPC cell lines, namely, TC411K and NCI-H660, as well as in human 22Rv1 adenocarcinoma cells. Results showed that, besides ST4787 cells, SDC1 was expressed by other murine and human NEPC cells (TC411K and NCI-H660) but not by human prostate adenocarcinoma cells (22Rv1; **Fig. 6E**). Conversely, none of the newly examined cell lines was positive for CD14, except for a tiny positivity observed in TC411K (Supplementary Fig. S9H). These data support the broad relevance of SDC1, but not of CD14, across different NEPC models.

Because we confirmed that TNFα-expressing MCs accumulated in incipient NEPC rather than in fully developed NEPC (**Fig. 5B** and **D**), we hypothesized that also SDC1, responsible for the activation of the TLR/MyD88/iOPN/TNFα pathway in MCs, needed to be expressed in the same time frame by NEPC cells. To prove this hypothesis, we analyzed a publicly available single-cell (sc) RNA-seq data set, generated in the TPPRC mouse model (inducible triple knockout for *Tp53*, *Rb1*, and *Pten*, driven by a luminal cell-specific, tamoxifen-inducible, Cre recombinase), which recapitulates all the transition stages of NEPC development (30). This data set comprehensively analyzed all the cells, comprising tumor and stromal, freshly isolated from the tumors at different time points (from 2 weeks to 6 months) after tamoxifen administration and consequent tumor development. Deconvolution of the scRNA-seq data identified 20 different clusters of cells along the different stages of NEPC development (**Fig. 6F**). Superimposing gene signatures specific for adenocarcinoma, NEPC, or MCs, we found that clusters 8 and 14 comprised adenocarcinoma cells. Clusters 11, 13, 3, and 15 were representative of cells in transition from adenocarcinoma to NEPC, because they concomitantly expressed adenocarcinoma and NEPC markers, albeit the levels of these markers were different in each of these clusters. Clusters 11 and 13 were also characterized by a high number of cells overexpressing *Sdc1*, which was also expressed by some cells in cluster 3. Conversely, in clusters 11, 13, 3, and 15, *Cd14* was expressed at low levels and only by a very small number of cells. We also associated cluster 17 with fully developed NEPC cells. Cluster 7 identified MCs, also expressing high levels of *Tlr2* and *Tnf*, and of *Tlr4*, albeit at a lower extent. In addition, we observed that this latter cluster co-existed with cluster 11, since 2.5 months of tumor development. Then, from 3.5 months, clusters 7, 3, and 15 seemed to be simultaneously present. Cluster 17, representative of the final stage of NEPC outgrowth, emerged at 6 months of tumor development, when cluster 7 faded (**Fig. 6F**).

This analysis suggests that the SDC1-TLR2/TLR4 interaction between incipient NEPC and MC that leads to TNFα production, can occur also in a different prostate cancer model, thus confirming the wide-ranging significance of the mechanism that we unveiled. Further, these data contributed to the use excluding the relevance of CD14 across different NEPC models.

SDC1 is expressed in mouse and human incipient NEPC

As a result of our demonstration of SDC1 consistent expression in various murine and human NEPC cells and models

(**Fig. 6A–E** and **F**), we decided to pursue further investigation of the transmembrane heparan sulfate proteoglycan SDC1 as the possible NEPC-specific ligand that activates the iOPN/MyD88/TNFα pathway in MCs. To increase the translational relevance of our results, we interrogated a human dataset that includes mCRPC specimens from patients who received ADT, and that, through extensive transcriptomic and immunohistochemistry analyses, classifies tumors into five different phenotypes, ranging from adenocarcinoma (ARPC, AR^+/NE^-) to fully developed NEPC (SNPC, AR^-/NE^+), passing through intermediate stages (AMPC, AR^+NE^+; ARLPC, AR^{low}/NE^-; DNPC, AR^-NE^-; ref. 29). According to our hypothesis, we found that *Sdc1* was upregulated in one of the intermediate, incipient, NEPC stages but was finally downregulated at the final stage of NEPC outgrowth (**Fig. 7A**). Further translational relevance of our results came from the detection of the SDC1 protein in incipient NEPC areas of tumor samples from castrated TRAMP mice (**Fig. 7B**) and from patients who underwent neoadjuvant ADT (**Fig. 7C**) but not in murine or human adenocarcinoma lesions (**Fig. 7B** and **C**).

In conclusion, our study indicates that MCs can inhibit NEPC outgrowth through the release of TNFα in response to SDC1, a specific stimulus expressed by incipient NEPC cells. The underlying mechanism reveals a role of iOPN in MCs, in which it binds to MyD88 to stimulate TLR2 and/or TLR4 signaling and consequent TNFα production. These results pave the way for new therapeutic strategies against NEPC aimed either to stimulate MC function toward TNFα production or to provide local delivery of TNFα. We also highlight SDC1 as a new potential biomarker for the detection of incipient NEPC.

Discussion

NEPC is a fatal disease that evolves from prostate adenocarcinoma relapsing to hormone therapies (t-NEPC), or, more rarely, is found at first diagnosis in untreated patients (*de novo* NEPC). Still, the urgent need for effective drugs for NEPC is hampered by the limited knowledge of the molecular mechanisms that regulate its growth.

Our study uncovers a mechanism involving MCs and the SDC1/TLR/MyD88/iOPN/TNFα axis that restrains the development of NEPC. It is known that MCs can exert pro- or antitumorigenic functions depending on tumor type and interactions with other cells in the tumor microenvironment (5). Yet, our findings are in line with previous literature showing the cytotoxic effects of MC-derived TNFα (38) and the association of TNFα-positive MCs to favorable prognosis in nasopharyngeal cancer (39). Our data showing that MCs restrain NEPC are also consistent with articles that suggest that intratumoral MCs can protect against prostate cancer recurrence (40, 41). Indeed, peri- or intra-tumor localization seems to determine the function of MCs in prostate cancer, as other studies indicate that peri-tumoral MCs can support tumor development and metastasis formation (42, 43). Yet, none of these cited articles specifically addressed the role of MCs in NEPC.

We also unveil a function of iOPN in MCs, in which iOPN can bind MyD88 promoting TLR2 and/or TLR4 signaling and consequent TNFα production. Our results are consistent with existing literature that shows that iOPN can stimulate TLR2 signaling in macrophages during fungal infections (16). However, it is noteworthy that in macrophages, iOPN can also inhibit the TLR4 pathway, thereby restricting inflammatory responses (33), and restraining the production of pro-inflammatory cytokines ultimately impeding the progression of liver cancer (14). Finally, iOPN can promote or inhibit TLR9 signaling in plasmacytoid dendritic cells or in malignant B cells, respectively (13, 15). However, we opted to exclude the involvement of TLR9 in the mechanism outlined in this manuscript, because TLR9 is an intracellular receptor activated by soluble ligands, and we showed with transwell experiments that MCs inhibited NEPC growth solely through direct contact. Indeed, our data point out the involvement of both TLR2 and TLR4 in the cross-talk between MCs and tumor cells that leads to TNFα production by MCs. We will dissect in future studies the relative contribution of TLR2 and TLR4 in this context. Future investigations are also required to define whether iOPN exerts additional functions in MCs, besides those described in this manuscript.

Furthermore, our experiments revealed that reconstitution with $OPN^{-/-}$ MCs, albeit not as efficient as WT MCs, can partially reduce the rate of NEPC in mice. This evidence lets us hypothesize that MCs can count also on OPN-independent mechanisms to restrain NEPC. Given that $OPN^{-/-}$ MCs do not affect NEPC growth *in vitro*, such additional MC functions are likely to be exerted through the recruitment/activation of other cells within the tumor microenvironment, and will be the subject of future studies as a follow-up of this manuscript.

Our findings showing that OPN is protective against NEPC seem at odds with previous studies reporting the harmful role of OPN in prostate cancer (44, 45). However, those studies addressed the role of tumor-derived, and secreted, OPN, whereas we specifically investigated MC-derived intracellular OPN. Nevertheless, our data are consistent with a previous publication that showed a protective role of host-derived OPN in prostate cancer, unveiling that, in TRAMP mice and in a TRAMP-derived transplantable model, sOPN can recruit NK cells to defeat tumor growth (46). However, despite using OPN-deficient TRAMP mice, as we did here, that study did not directly address the adenocarcinoma or NEPC histotype of tumors developed in the absence of OPN (46).

We show here that TNFα produced by MCs can specifically target and restrain NEPC cells while sparing prostate adenocarcinoma. Furthermore, in this work, we found that MCs selectively produce TNFα in response to SDC1 expressed by NEPC cells, *in vitro*, and in incipient NEPC areas in mouse and patient-derived specimens. Nevertheless, as shown both here and in our previous publications (6, 8), while MCs are enriched in prostate adenocarcinoma, they drop in fully developed NEPC. Similarly, the key molecules involved in the network that we unveiled in this study (TNFα and SDC1) are upregulated at the stage of incipient NEPC or during the first steps of NEPC development but lost in fully developed NEPC. Based on these observations, we propose that the effectiveness of MCs against NEPC is limited to the initial and intermediate phases of NEPC development. Within this specific time frame, MCs actively oppose NEPC growth. However, when NEPC progresses toward full outgrowth, we postulate that MCs need to be either excluded, inhibited, or even eliminated due to microenvironmental modifications occurring during the process. Understanding these hypothetical mechanisms of NEPC escape from MCs will be the focus of future investigations.

Our findings have implications for the development of therapeutic strategies for NEPC patients. We propose that the adoptive transfer of MCs following ADT/ARPI could be a promising approach to mitigate the occurrence of t-NEPC. Furthermore, the foreseen in-depth investigation into the mechanisms governing MC clearance in NEPC becomes of paramount importance, as it could

provide insights into how to restore MC homing or enhance their activity at the tumor site. However, when evaluating all these strategies, it becomes essential to give careful consideration to avoid inadvertently fostering residual adenocarcinoma, as we are aware that MCs can promote its growth (6, 7).

A more powerful approach could consist of the administration of TLR2 and/or TLR4 agonists as adjuvant immunotherapy in patients receiving ADT/ARPI treatment, to specifically trigger TNFα release by tumor-infiltrating MCs. Interestingly, previous research proved that the synthetic agonist Pam_3CSK_4 can activate TLR2 on MCs, thereby hampering tumor growth in a mouse model of melanoma (47). However, whereas immunotherapy with agonists of TLR7, TLR8, TLR9, and TLR3 has been extensively investigated in patients, a tiny number of clinical studies have been reported for TLR2 agonists. An exception is represented by Bacille Calmette-Guérin, a living mycobacteria that can activate TLR2 and TLR4, which is standard of care therapy for high-risk bladder cancer patients, administered as adjuvant after the surgical removal of the tumor (48). Furthermore, phase 2 clinical trials assessing the effectiveness of two different TLR2 agonists, namely CBLB612 and ISA-20, as potential cancer therapies have been carried out (study identifiers NCT02778763 and NCT02821494, respectively). However, the outcomes of these trials have not been disclosed yet, and information about potential toxicity or side effects remains unavailable. Furthermore, when evaluating the effect of this kind of immunotherapy, it should be kept in mind that the outcome could be influenced by the fact that several types of immune cells and even tumor cells can express TLR2 and TLR4.

Alternatively, our results highlight that TNFα administration holds promise as a valuable therapeutic approach for NEPC. Nevertheless, the systemic delivery of TNFα is linked to considerable toxicity (49), making it unsuitable for current clinical use. To overcome this limitation, the development of a NEPC-specific targeted delivery system for TNFα could represent a potential opportunity to reduce systemic toxicity while enhancing the efficacy of TNFα treatment.

Finally, our identification of SDC1 as selectively over-expressed by incipient NEPC may suggest a possible role for SDC1 as a biomarker for the detection of incipient NEPC. Even if we did not find any published study that specifically addresses SDC1 expression in NEPC, our data are in accordance with literature showing that in prostate cancer patients SDC1 is upregulated in tumors with a high Gleason score (4 + 5; refs. 50, 51) and following ADT (52). Furthermore, it has to be noticed that SDC1 was found highly expressed in soft-tissue metastasis but not in bone metastasis in prostate cancer patients (53). This result is interesting considering that NEPC preferentially develops in visceral metastases (24). It is also worth mentioning that SDC1 expression in tissues and/or levels of circulating SDC1 have already been proposed as prognostic biomarkers, correlating with poor prognosis, relapse, and chemotherapy resistance in prostate cancer patients (50, 53–55). Nevertheless, none of these studies investigated the correlation between SDC1 expression and NEPC outcome.

In conclusion, our findings provide valuable insights into the molecular mechanisms underlying NEPC development and highlight the importance of iOPN-mediated signaling in MCs, paving the way for future therapeutic interventions. Furthermore, the identification of the preferential overexpression of SDC1 by incipient NEPC foresees the possibility to utilize it as a biomarker for early detection of this lethal form of prostate cancer.

Authors' Disclosures

E. Jachetti reports grants from Italian Ministry of Health and grants from Associazione Italiana per la Ricerca sul Cancro (AIRC) during the conduct of the study. No disclosures were reported by the other authors.

Authors' Contributions

R. Sulsenti: Conceptualization, investigation, visualization, methodology, writing–original draft, writing–review and editing. **G.B. Scialpi:** Investigation, visualization. **B. Frossi:** Investigation, methodology, writing–original draft, writing–review and editing. **L. Botti:** Investigation. **R. Ferri:** Investigation. **I. Tripodi:** Formal analysis. **A. Piva:** Formal analysis. **S. Sangaletti:** Investigation. **D. Pernici:** Formal analysis. **V. Cancila:** Investigation. **F. Romeo:** Investigation, methodology. **C. Chiodoni:** Resources, investigation. **D. Lecis:** Resources, investigation. **F. Bianchi:** Investigation, methodology. **I. Fischetti:** Investigation. **C. Enriquez:** Investigation. **F. Crivelli:** Resources. **M. Bregni:** Resources. **G. Renne:** Resources. **S. Pece:** Resources. **C. Tripodo:** Investigation. **C.E. Pucillo:** Writing–original draft, writing–review and editing. **M.P. Colombo:** Conceptualization, supervision, writing–original draft, writing–review and editing. **E. Jachetti:** Conceptualization, supervision, funding acquisition, visualization, methodology, writing–original draft, writing–review and editing.

Acknowledgments

This work was supported by Grants from the Italian Ministry of Health (GR-2016-02362484 to E. Jachetti and "Ricerca Corrente Funds") and Fondazione AIRC per la Ricerca sul Cancro (AIRC; Investigator Grant 25854 to E. Jachetti). The authors declare no competing financial interests. We thank Francesco Crea (The Open University, Milton Keynes, UK) for the kind provision of LASCPC-01 cells, which he purchased from ATCC; Luigina Romani (University of Perugia, Italy) for the kind provision of tibiae and femurs from $MyD88^{-/-}$ mice; M.L. Shinohara (Duke University School of Medicine, Durham, NC, USA), for providing the cDNA of iOPN. We also thank from Fondazione IRCCS Istituto Nazionale dei Tumori: Gabriella Abolafio for cell sorting, Paolo Verderio, and Mara Lecchi for sample size calculation in murine experiments, Loris De Cecco and Edoardo Marchesi for microarray analysis and Ester Grande for administrative assistance.

Note

Supplementary data for this article are available at Cancer Immunology Research Online (http://cancerimmunolres.aacrjournals.org/).

Received September 25, 2023; revised March 28, 2024; accepted June 11, 2024; published first June 12, 2024.

References

1. Sung H, Ferlay J, Siegel RL, Laversanne M, Soerjomataram I, Jemal A, et al. Global cancer statistics 2020: GLOBOCAN estimates of incidence and mortality worldwide for 36 cancers in 185 countries. CA Cancer J Clin 2021;71:209–49.
2. Aggarwal R, Huang J, Alumkal JJ, Zhang L, Feng FY, Thomas GV, et al. Clinical and genomic characterization of treatment-emergent small-cell neuroendocrine prostate cancer: a multi-institutional prospective study. J Clin Oncol 2018;36:2492–503.
3. Chedgy EC, Vandekerkhove G, Herberts C, Annala M, Donoghue AJ, Sigouros M, et al. Biallelic tumour suppressor loss and DNA repair defects in de novo small-cell prostate carcinoma. J Pathol 2018;246:244–53.
4. Beltran H, Hruszkewycz A, Scher HI, Hildesheim J, Isaacs J, Yu EY, et al. The role of lineage plasticity in prostate cancer therapy resistance. Clin Cancer Res 2019;25:6916–24.
5. Sulsenti R, Jachetti E. Frenemies in the microenvironment: harnessing mast cells for cancer immunotherapy. Pharmaceutics 2023;15:1692.

6. Pittoni P, Tripodo C, Piconese S, Mauri G, Parenza M, Rigoni A, et al. Mast cell targeting hampers prostate adenocarcinoma development but promotes the occurrence of highly malignant neuroendocrine cancers. Cancer Res 2011; 71:5987–97.
7. Jachetti E, Cancila V, Rigoni A, Bongiovanni L, Cappetti B, Belmonte B, et al. Cross-talk between myeloid-derived suppressor cells and mast cells mediates tumor-specific immunosuppression in prostate cancer. Cancer Immunol Res 2018;6:552–65.
8. Jachetti E, Rigoni A, Bongiovanni L, Arioli I, Botti L, Parenza M, et al. Imatinib spares cKit-expressing prostate neuroendocrine tumors, whereas kills seminal vesicle epithelial-stromal tumors by targeting PDGFR-β. Mol Cancer Ther 2017;16:365–75.
9. Mauri G, Jachetti E, Comuzzi B, Dugo M, Arioli I, Miotti S, et al. Genetic deletion of osteopontin in TRAMP mice skews prostate carcinogenesis from adenocarcinoma to aggressive human-like neuroendocrine cancers. Oncotarget 2016;7:3905–20.
10. Castello LM, Raineri D, Salmi L, Clemente N, Vaschetto R, Quaglia M, et al. Osteopontin at the crossroads of inflammation and tumor progression. Mediators Inflamm 2017;2017:4049098.
11. Shinohara ML, Kim HJ, Kim JH, Garcia VA, Cantor H. Alternative translation of osteopontin generates intracellular and secreted isoforms that mediate distinct biological activities in dendritic cells. Proc Natl Acad Sci U S A 2008; 105:7235–9.
12. Lin EY-H, Xi W, Aggarwal N, Shinohara ML. Osteopontin (OPN)/SPP1: from its biochemistry to biological functions in the innate immune system and the central nervous system (CNS). Int Immunol 2023;35:171–80.
13. Shinohara ML, Lu L, Bu J, Werneck MB, Kobayashi KS, Glimcher LH, et al. Osteopontin expression is essential for interferon-alpha production by plasmacytoid dendritic cells. Nat Immunol 2006;7:498–506.
14. Fan X, He C, Jing W, Zhou X, Chen R, Cao L, et al. Intracellular Osteopontin inhibits toll-like receptor signaling and impedes liver carcinogenesis. Cancer Res 2015;75:86–97.
15. Rizzello C, Cancila V, Sangaletti S, Botti L, Ratti C, Milani M, et al. Intracellular osteopontin protects from autoimmunity-driven lymphoma development inhibiting TLR9-MYD88-STAT3 signaling. Mol Cancer 2022;21:215.
16. Inoue M, Moriwaki Y, Arikawa T, Chen YH, Oh YJ, Oliver T, et al. Cutting edge: critical role of intracellular osteopontin in antifungal innate immune responses. J Immunol 2011;186:19–23.
17. Greenberg NM, DeMayo F, Finegold MJ, Medina D, Tilley WD, Aspinall JO, et al. Prostate cancer in a transgenic mouse. Proc Natl Acad Sci U S A 1995;92: 3439–43.
18. Grimbaldeston MA, Chen CC, Piliponsky AM, Tsai M, Tam SY, Galli SJ. Mast cell-deficient W-sash c-kit mutant kit W-sh/W-sh mice as a model for investigating mast cell biology *in vivo*. Am J Pathol 2005;167:835–48.
19. Gilmour DT, Lyon GJ, Carlton MB, Sanes JR, Cunningham JM, Anderson JR, et al. Mice deficient for the secreted glycoprotein SPARC/osteonectin/BM40 develop normally but show severe age-onset cataract formation and disruption of the lens. EMBO J 1998;17:1860–70.
20. Sulsenti R, Frossi B, Bongiovanni L, Cancila V, Ostano P, Fischetti I, et al. Repurposing of the antiepileptic drug levetiracetam to restrain neuroendocrine prostate cancer and inhibit mast cell support to adenocarcinoma. Front Immunol 2021;12:622001.
21. Nabel G, Galli SJ, Dvorak AM, Dvorak HF, Cantor H. Inducer T lymphocytes synthesize a factor that stimulates proliferation of cloned mast cells. Nature 1981;291:332–4.
22. Nilsson G, Blom T, Kusche-Gullberg M, Kjellen L, Butterfield JH, Sundstrom C, et al. Phenotypic characterization of the human mast-cell line HMC-1. Scand J Immunol 1994;39:489–98.
23. Enriquez C, Cancila V, Ferri R, Sulsenti R, Fischetti I, Milani M, et al. Castration-induced downregulation of SPARC in stromal cells drives neuroendocrine differentiation of prostate cancer. Cancer Res 2021;81:4257–74.
24. Beltran H, Tomlins S, Aparicio A, Arora V, Rickman D, Ayala G, et al. Aggressive variants of castration-resistant prostate cancer. Clin Cancer Res 2014; 20:2846–50.
25. Beltran H, Prandi D, Mosquera JM, Benelli M, Puca L, Cyrta J, et al. Divergent clonal evolution of castration-resistant neuroendocrine prostate cancer. Nat Med 2016;22:298–305.
26. Cerami E, Gao J, Dogrusoz U, Gross BE, Sumer SO, Aksoy BA, et al. The cBio cancer genomics portal: an open platform for exploring multidimensional cancer genomics data. Cancer Discov 2012;2:401–4.
27. Gao J, Aksoy BA, Dogrusoz U, Dresdner G, Gross B, Sumer SO, et al. Integrative analysis of complex cancer genomics and clinical profiles using the cBioPortal. Sci Signal 2013;6:pl1.
28. Phipson B, Lee S, Majewski IJ, Alexander WS, Smyth GK. Robust hyperparameter estimation protects against hypervariable genes and improves power to detect differential expression. Ann Appl Stat 2016;10: 946–63.
29. Labrecque MP, Coleman IM, Brown LG, True LD, Kollath L, Lakely B, et al. Molecular profiling stratifies diverse phenotypes of treatment-refractory metastatic castration-resistant prostate cancer. J Clin Invest 2019;129: 4492–505.
30. Han M, Li F, Zhang Y, Dai P, He J, Li Y, et al. FOXA2 drives lineage plasticity and KIT pathway activation in neuroendocrine prostate cancer. Cancer Cell 2022;40:1306–23.e8.
31. Inoue M, Shinohara ML. Intracellular osteopontin (iOPN) and immunity. Immunol Res 2011;49:160–72.
32. Kanayama M, Xu S, Danzaki K, Gibson JR, Inoue M, Gregory SG, et al. Skewing of the population balance of lymphoid and myeloid cells by secreted and intracellular osteopontin. Nat Immunol 2017;18:973–84.
33. Yang H, Ye X, Zhang X, Li X, Fu Q, Tang Z. Intracellular osteopontin negatively regulates toll-like receptor 4-mediated inflammatory response via regulating GSK3β and 4EBP1 phosphorylation. Cytokine 2018;108:89–95.
34. Lee CC, Avalos AM, Ploegh HL. Accessory molecules for Toll-like receptors and their function. Nat Rev Immunol 2012;12:168–79.
35. Sandig H, Bulfone-Paus S. TLR signaling in mast cells: common and unique features. Front Immunol 2012;3:185.
36. Laster SM, Wood JG, Gooding LR. Tumor necrosis factor can induce both apoptic and necrotic forms of cell-lysis. J Immunol 1988;141:2629–34.
37. Armingol E, Officer A, Harismendy O, Lewis NE. Deciphering cell-cell interactions and communication from gene expression. Nat Rev Genet 2021;22: 71–88.
38. Bischoff SC, Lorentz A, Schwengberg S, Weier G, Raab R, Manns MP. Mast cells are an important cellular source of tumour necrosis factor alpha in human intestinal tissue. Gut 1999;44:643–52.
39. Cheng S, Li Z, Gao R, Xing B, Gao Y, Yang Y, et al. A pan-cancer single-cell transcriptional atlas of tumor infiltrating myeloid cells. Cell 2021;184:792–809. e23.
40. Hempel HA, Cuka NS, Kulac I, Barber JR, Cornish TC, Platz EA, et al. Low intratumoral mast cells are associated with a higher risk of prostate cancer recurrence. Prostate 2017;77:412–24.
41. Fleischmann A, Schlomm T, Kollermann J, Sekulic N, Huland H, Mirlacher M, et al. Immunological microenvironment in prostate cancer: high mast cell densities are associated with favorable tumor characteristics and good prognosis. Prostate 2009;69:976–81.
42. Hempel Sullivan H, Heaphy CM, Kulac I, Cuka N, Lu J, Barber JR, et al. High extratumoral mast cell counts are associated with a higher risk of adverse prostate cancer outcomes. Cancer Epidemiol Biomarkers Prev 2020; 29:668–75.
43. Johansson A, Rudolfsson S, Hammarsten P, Halin S, Pietras K, Jones J, et al. Mast cells are novel independent prognostic markers in prostate cancer and represent a target for therapy. Am J Pathol 2010;177:1031–41.
44. Castellano G, Malaponte G, Mazzarino MC, Figini M, Marchese F, Gangemi P, et al. Activation of the osteopontin/matrix metalloproteinase-9 pathway correlates with prostate cancer progression. Clin Cancer Res 2008;14: 7470–80.
45. Khodavirdi AC, Song Z, Yang S, Zhong C, Wang S, Wu H, et al. Increased expression of osteopontin contributes to the progression of prostate cancer. Cancer Res 2006;66:883–8.
46. Danzaki K, Kanayama M, Alcazar O, Shinohara ML. Osteopontin has a protective role in prostate tumor development in mice. Eur J Immunol 2016;46: 2669–78.
47. Oldford SA, Haidl ID, Howatt MA, Leiva CA, Johnston B, Marshall JS. A critical role for mast cells and mast cell-derived IL-6 in TLR2-mediated inhibition of tumor growth. J Immunol 2010;185:7067–76.
48. Cole K, Al-Kadhimi Z, Talmadge JE. Highlights into historical and current immune interventions for cancer. Int Immunopharmacol 2023;117: 109882.
49. Gamm H, Lindemann A, Mertelsmann R, Herrmann F. Phase I trial of recombinant human tumour necrosis factor alpha in patients with advanced malignancy. Eur J Cancer 1991;27:856–63.

50. Zellweger T, Ninck C, Mirlacher M, Annefeld M, Glass AG, Gasser TC, et al. Tissue microarray analysis reveals prognostic significance of syndecan-1 expression in prostate cancer. Prostate 2003;55:20–9.
51. Martini C, Logan JM, Sorvina A, Gordon C, Beck AR, Ung BS-Y, et al. Aberrant protein expression of Appl1, Sortilin and Syndecan-1 during the biological progression of prostate cancer. Pathology 2023;55:40–51.
52. Shimada K, Nakamura M, De Velasco MA, Tanaka M, Ouji Y, Konishi N. Syndecan-1, a new target molecule involved in progression of androgen-independent prostate cancer. Cancer Sci 2009;100:1248–54.
53. Chen D, Adenekan B, Chen L, Vaughan ED, Gerald W, Feng Z, et al. Syndecan-1 expression in locally invasive and metastatic prostate cancer. Urology 2004;63:402–7.
54. Kind S, Kluth M, Hube-Magg C, Moller K, Makrypidi-Fraune G, Lutz F, et al. Increased cytoplasmic CD138 expression is associated with aggressive characteristics in prostate cancer and is an independent predictor for biochemical recurrence. Biomed Res Int 2020;2020:5845374.
55. Szarvas T, Sevcenco S, Modos O, Keresztes D, Nyirady P, Kubik A, et al. Circulating syndecan-1 is associated with chemotherapy-resistance in castration-resistant prostate cancer. Urol Oncol 2018;36:312.e9–15.